Geological Quarterly, 2024, 68, 45
DOI: http://dx.doi.org/10.7306/gq.1773

Origin and evolution of heavy mineral assemblages of the Late Cretaceous Szozdy Delta System (Polish Cretaceous Basin): insights into burial history, weathering processes and parent rocks

Michał CYGLICKI[1, 2, *] and Zbyszek REMIN[2]

[1] Polish Geological Institute – National Research Institute, Rakowiecka 4, 00-975 Warszawa, Poland; ORCID: 0000-0002-1146-8042 [M.C.]

[2] University of Warsaw, Faculty of Geology, Żwirki i Wigury 93, 02-089 Warszawa, Poland; ORCID: 0000-0003-4159-0126 [Z.R.]

Cyglicki, M., Remin, Z., 2024. Origin and evolution of heavy mineral assemblages of the Late Cretaceous Szozdy Delta System (Polish Cretaceous Basin): insights into burial history, weathering processes and parent rocks. Geological Quarterly, 68, 45; https://doi.org/10.7306/gq.1773

During the Late Cretaceous, inversion tectonics affected basins across Europe; in Poland, the axial part of the Polish Basin – the Mid-Polish Trough – was uplifted and transformed into one of the most prominent Mesozoic structures of Europe – the Mid-Polish Anticlinorium, with the Lower San Anticlinorium forming its supposed southeastern extension. For decades, the axial part of the Polish Basin was considered to represent the deepest, most rapidly subsiding part of the basin during the Mesozoic times, simultaneously being filled by deposits of that age. The recently defined Łysogóry-Dobrogea Land in the heart of the then-inverting axial part of the Polish Cretaceous Basin (the present-day subsurface Lower San Anticlinorium) overturned this framework. Moreover, the discovery of the Late Cretaceous Szozdy Delta System on the northern peripheries of Łysogóry-Dobrogea Land shed new light on the palaeogeography and tectonic evolution of the southeastern part of the Polish Basin – a part of the trans-European Basin System that developed over a major part of epicratonic Europe. It clearly appears that, during the Late Cretaceous, this area should be considered as an emergent landmass supplying the Szozdy Delta System, instead of as the deepest part of the basin. Although the prominent quartz sand input into the Cretaceous deposits of the Roztocze Hills is a well-known phenomenon, it has never been explored to reveal the potential parent rocks and possible degree of burial. To fill this gap, we have analysed the heavy mineral assemblages from the Szozdy Delta System, demonstrating their truly polycyclic nature. High ZTR (zircon, tourmaline, rutile) index values, the high degree of roundness, and the presence of some grain surface textures reflecting abrasion indicates multiple rounds of redeposition. However, the assemblages also include predominantly angular grains of minerals which are less resistant to erosion, which is inconsistent with repeated redeposition. Accordingly, the data suggest at least two distinct sources were involved. The first comprised multi-recycled mineral phases dominated by minerals of ZTR group, for which the source might be metapelites and/or metapsammites. The second “fresh” source delivered angular garnet, kyanite and staurolite grains, for which metamorphosed rocks were the main source. Such characteristics would be difficult to obtain from the suggested Mesozoic sedimentary cover of the San Anticlinorium (if a Mesozoic cover was even present), necessitating a search for other sources. Thus, these heavy mineral assemblages suggest a different burial history than previously assumed.

Key words: Late Cretaceous, inversion tectonics, Szozdy Delta System, sedimentology, heavy minerals, provenance, burial history.

INTRODUCTION

During the Late Cretaceous, central Europe was affected by compressional tectonics, resulting in basement uplift and basin inversion across the entire Central European Basin System (e.g., Ziegler, 1990; Nielsen and Hansen, 2000; Krzywiec, 2006; Kley and Voigt, 2008; Krzywiec and Stachowska, 2016; Voigt et al., 2021). Marked changes in palaeogeography, and especially facies architecture, induced by Late Cretaceous inversion tectonics, are particularly identifiable along the margin of the East European Craton (Figs. 1 and 2; Krzywiec et al., 2009, 2018; Remin et al., 2016, 2022a, b; Remin, 2018).

The present-day Roztocze Hills (which host the Szozdy Delta System) in the Late Cretaceous times constituted the axial part of the Polish Basin – that is, the Mid-Polish Trough. During inversion, it was uplifted and transformed into one of the most prominent Mesozoic structural units in Europe – the Mid-Polish Anticlinorium (Fig. 2; for a thorough reviews, see: Krzywiec et al., 2009, 2018; Walaszczyk and Remin, 2015; Remin et al., 2022a, b).

Although the timing of inversion onset has long been debated, it is now considered to have initiated in late Turonian/Coniacian times (e.g., Pożaryski, 1960, 1962; Jaskowiak-Schoeneichowa and Krassowska, 1988; Walaszczyk, 1992;

* Corresponding author, e-mail: mcyglicki@uw.edu.pl

Received: December 22, 2022; accepted: November 26, 2024; first published online: December 31, 2024

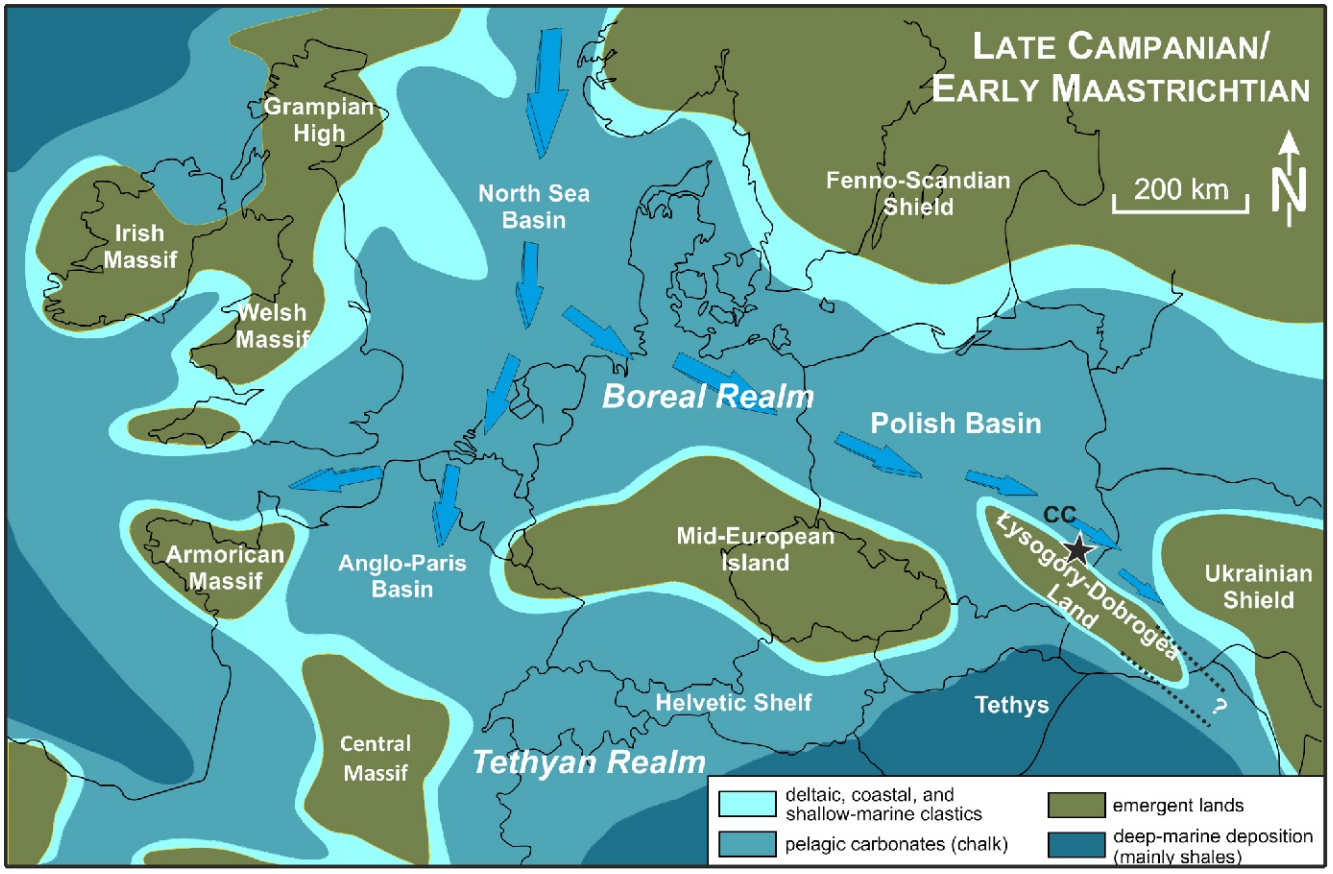

Fig. 1. Schematic palaeogeographic map (compiled from Ziegler, 1990; Dadlez et al., 1998), and location of the section studied in southeastern Poland (marked with a black star)

Ocean currents are based on Remin et al. (2016) and Remin (2018); figure adapted from Remin et al. (2022a, b)

Leszczyński and Dadlez, 1999; Krzywiec et al., 2009, 2018; Leszczyński, 2010, 2012; Walaszczyk and Remin, 2015; Remin et al., 2016, 2022a, b; Remin, 2018; Łuszczak et al., 2020).

However, starting from the early 1970s, Kutek and Głazek (1972) provided a palaeotectonic model which for decades dominated thinking about the Mesozoic palaeotectonic evolution of the Polish Basin, placing the onset of inversion processes as late as in the Maastrichtian. In their model the southeastern part of the Polish Basin, the Mid-Polish Trough, was considered to represent the axial, deepest and the most rapidly subsiding part of the basin (e.g., Kutek and Głazek, 1972; Hakenberg and Świdrowska, 1998, 2001; Świdrowska and Hakenberg, 1999; Świdrowska, 2007; Świdrowska et al., 2008). For that reason, the Campanian and Maastrichtian deposits of the Roztocze Hills, represented mainly by opokas, sandy and marly opokas, (siliceous chalk/limestone with a variable admixture of biogenic silica), and gaizes (siliceous limestone with a considerable admixture of detrital quartz, glaucony, and clay; for a full account, cf. Remin et al., 2022a, b), and sandy/muddy limestone, were considered to represent deep, shelf-type deposits (e.g., Hakenberg and Świdrowska, 1998; Świdrowska, 2007). Additionally, this implied that areas of the Mid-Polish Anticlinorium, currently devoid of Mesozoic remnants (Fig. 2), were deeply buried and covered by thick Mesozoic deposits (discussion in Remin et al., 2022a, b). Despite this, some of the authors continued to maintain that the axial part of the Mid-Polish Trough during the Turonian-Maastrichtian constituted a shallower area of the basin (e.g., Jaskowiak-Schoeneichowa and Krassowska, 1988; Krassowska, 1997; Leszczyński and Dadlez, 1999) what was subsequently clearly demonstrated and corroborated by interpretation of seimic profiles (Krzywiec et al., 2009, 2018).

The discovery of the middle Campanian (Late Cretaceous) Szozdy Delta System (Remin et al., 2022a) on the northern peripheries of Łysogóry-Dobrogea Land shed new light on the palaeogeography and tectonic evolution of the southeastern part of the Polish Cretaceous Basin – a part of the trans-European Basin System that developed during the Late Cretaceous over most of epicratonic Europe.

After the discovery of the Szozdy Delta System (Remin et al., 2022a) in the heart of the Polish Basin, it became clear that the axial part of the Polish Basin should be considered as an emergent landmass or palaeomorphological barrier i.e. as Łysogóry-Dobrogea Land rather than as the deepest part of the basin, at least from the Coniacian/Santonian onwards (Remin et al., 2016), or potentially even from the late Turonian (for review, compare: Krzywiec et al., 2009, 2018; Remin et al., 2022a, b).

Intriguingly, such an interpretation is not novel. Starting from the beginning of the 20th century, and indeed up until the 1960s and even later (e.g., Nowak, 1907, 1908; Rogala, 1909; Kamieński, 1925; Samsonowicz, 1925; Pożaryski, 1960, 1962), the area of southeast Poland was considered as an emergent landmass during the Late Cretaceous. Several different names were adopted for this landmass: "Łysogóry-Dobrogea Land" of Samsonowicz (1925), compare also Jurkowska et al. (2019a,

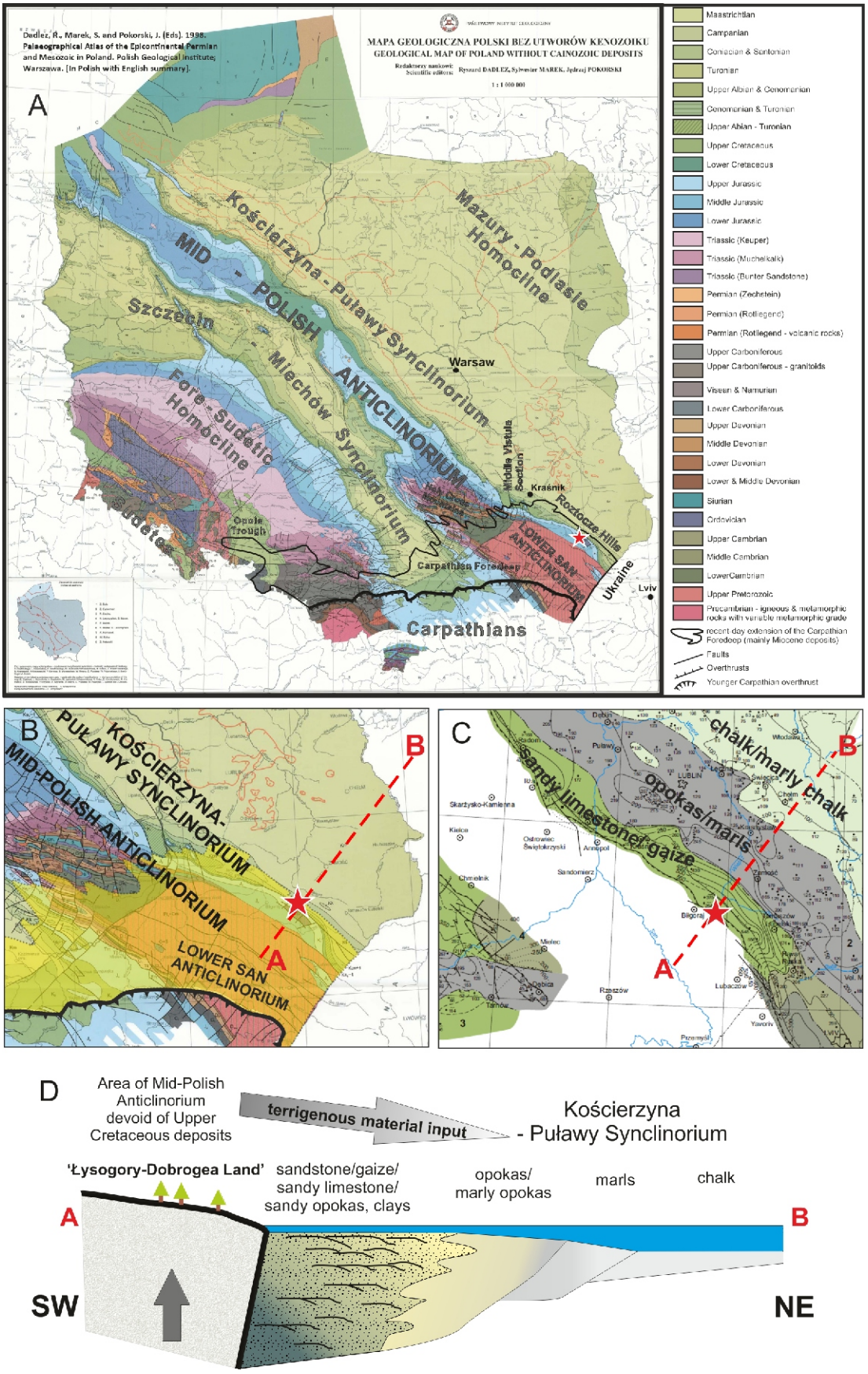

Fig. 2. Geological setting of the study area

A – location (marked with a red star) on the geological map of extra-Carpathian Poland, excluding Cenozoic deposits, except for the modern extension of the Carpathian Foredeep, adapted from Dadlez et al. (2000), tectonic units after Żelaźniewicz et al. (2011); **B** – detailed map, relative to the position of the Holy Cross Mountains (HCM) and the Lower San Anticlinorium; **C** – general distribution of Campanian lithofacies in SE Poland (adapted from Świdrowska, 2007); **D** – depositional, structural, and environmental interpretation of facies and bathymetry in a cross-section perpendicular to the axis of the Mid-Polish Anticlinorium (adapted from Remin et al. 2015a, 2022a, b; Walaszczyk and Remin, 2015)

b); the "Maastrichtian island" (Jurkowska and Barski, 2017); the "Krukienic Island" of Pasternak (1959), Pasternak et al. (1968, 1987), Walaszczyk (1992), Dubicka et al. (2014) and the "Świętokrzyski Land" or "Małopolska Land" of Pożaryski (1960, 1962) and Jaskowiak-Schoeneichowa and Krassowska (1988) and Krassowska (1997), among others.

The cyclic nature of the Szozdy succession is unique both for the Roztocze Hills and for other regions of the epicontinental Polish Cretaceous Basin. This discovery provided a fresh look at several fundamental aspects concerning the degree of burial, facies distribution, and palaeotectonic evolution of the southeastern part of the Central European Basin System. The source area that supplied terrestrial material to the Szozdy Delta System, was postulated (Remin et al., 2022a) to be located in the area of the present-day position of the Lower San Anticlinorium (the southeastern extension of the Mid-Polish Anticlinorium; Fig. 2), which currently is almost devoid of Mesozoic remnant deposits (Fig. 2).

However, beyond the existence of this Cretaceous landmass, little is known about it, particularly with regard to its potential overburden (if any such was present at all) and the nature of the exposed, eroding lithologies – that is, the source rocks. It may have been largely composed of the Mesozoic cover of the Lower San Anticlinorium. Alternatively, as we recently hypothesized (Remin et al., 2022a, b), older rocks, potentially even the Neoproterozoic-Cambrian basement beneath the Miocene cover of the Carpathian Foredeep (Fig. 2), may have already been eroded during the Late Cretaceous.

The primary rationale for this study is to clarify the nature of the overburden and parent rocks. To solve this problem and to gain insight into the source rocks and palaeogeographic context of Łysogóry-Dobrogea Land, which supplied terrigenous-rich material to the Szozdy Delta System, we studied heavy mineral assemblages (HMAs).

Heavy mineral analysis is a commonly used technique to discern source rock and provenance for siliciclastic deposits. The large variety of heavy minerals in sedimentary rocks and their limited paragenesis allows for the identification of parent rocks (e.g., Mange and Maurer, 1992; Morton and Hallsworth, 1999). The final heavy mineral suite depends on the rate of erosion, mineral density, sorting during transportation and/or deposition by currents, *in situ* dissolution, and the stability of individual phases during burial diagenesis (Komar, 2007; Morton and Hallsworth, 2007; Van Loon and Mange, 2007).

The extension of conventional methods combined with detailed dissolution structure classifications enables the correlation of seemingly monotonous sedimentary sequences and provides insight into palaeoclimate and/or diagenetic conditions (Mange-Rajetzky, 1995; Andò et al., 2012), that might have affected the source rocks during the Late Cretaceous. Electron microprobe analysis (EPMA) can yield additional valuable data as regards major element composition. The unique chemical composition of individual garnet and tourmaline grains can be diagnostic for the nature of the parent rock, providing invaluable data in provenance studies (Mange and Morton, 2007).

Our paper contributes to the identification of the parental rocks for Upper Cretaceous siliciclastic deposits of the Roztocze Hills. The unique heavy mineral assemblage we obtained suggests that pre-Mesozoic rocks were already being eroded during the Late Cretaceous, supplying the Szozdy Delta System.

REGIONAL SETTING

The Polish Basin, with the Mid-Polish Trough located at its most subsiding, axial part, represented the eastern part of the trans-European Basin System, collectively formed during the Permian and Mesozoic. From the Permian to the early Late Cretaceous, the Polish Basin experienced long-term subsidence (Dadlez et al., 1995). As a result, up to ~8000 m of Permian and Mesozoic deposits are present in the central part of the basin, especially along the NW–SE trending Mid-Polish Trough (e.g., Dadlez et al., 1998).

During the Late Cretaceous, the axial part of the Polish Basin – the Mid-Polish Trough – underwent uplift, inversion, and transformation into a prominent structural unit – the Mid-Polish Anticlinorium. Inversion tectonics started in the Late Turonian and lasted until the end of the Maastrichtian (and potentially into post-Maastrichtian times; e.g., Pożaryski, 1960, 1962; Krzywiec, 2000, 2002, 2006, 2009; Resak et al., 2008; Krzywiec et al., 2009, 2018; Remin et al., 2022a, b).

In south-east Poland (the study area), the middle/upper Albian (Lower Cretaceous) and Upper Cretaceous successions together comprise ~1000 m of deposits deposited in a rather shallow epicontinental basin (e.g., Jaskowiak-Schoeneich and Krassowska, 1988; Krassowska, 1997; Leszczyński, 2010, 2012). Outcrop and borehole data enable precise biostratigraphic subdivisions based on various taxonomic groups (cf. Walaszczyk et al., 2016; Remin et al., 2022b) and correlations with other regions both in Poland and beyond.

THE ROZTOCZE HILLS REGION

The Roztocze Hills form a range ~185 long by 25 km across between Kraśnik (southeast Poland) and Lviv (western Ukraine; Figs. 2 and 3). They are located to the northeast of, and run parallel to, the structurally elevated Mid-Polish Anticlinorium. To the southwest, the Roztocze Hills border the Carpathian Foredeep, which is filled with Miocene deposits (Dziadzio et al., 2006) and the subsurface San Anticlinorium (the southeastern part of the Mid-Polish Anticlinorium; Figs. 2 and 3). The pre-Miocene cover of the San Anticlinorium is almost entirely devoid of Mesozoic remnants (with a few exceptions; see Fig. 2) and is represented mainly by Cambrian and Neoproterozoic rocks, strongly tectonized and weakly metamorphosed comprising anchimetamorphic flysch-type deposits of unknown thickness (e.g., Dziadzio and Jachowicz, 1996; Buła et al., 2008; Żelaźniewicz et al., 2009; Buła and Habryn, 2011).

The Roztocze Hills are located on a fault zone (review in Narkiewicz et al., 2015; Narkiewicz and Petecki, 2017) that was repeatedly reactivated during the Late Cretaceous (Krzywiec, 1999; Krzywiec et al., 2009) and the Miocene, the latter during Carpathian movements (Kowalska et al., 2000; Buła et al., 2008; Buła and Habryn, 2011).

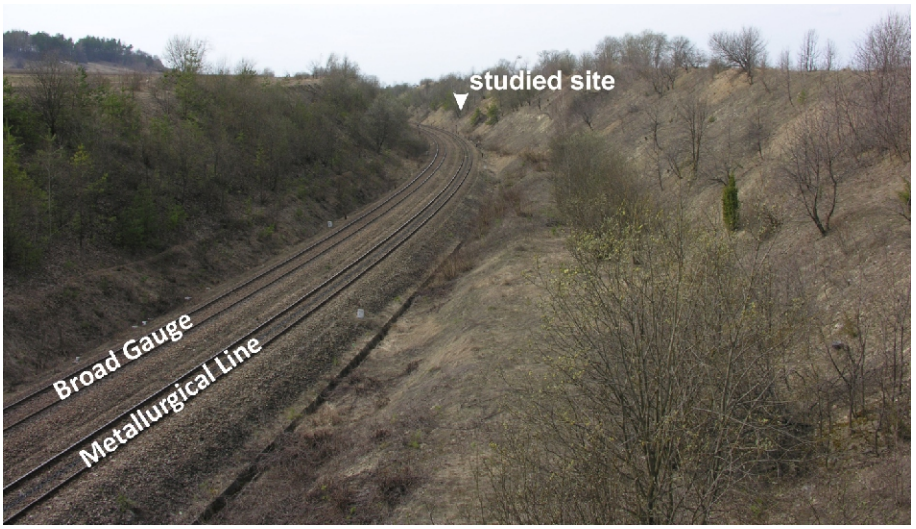

Fig. 3. General view of the Szozdy section

The exposures extend along both sides of the railway cutting over a distance of ~800 m (adapted from **Remin et al., 2022a**)

The Cretaceous of the Roztocze Hills is mainly represented by Campanian (~550 m thick) and Maastrichtian (~250 m, but incomplete) deposits that dip gently to the northeast. The older rocks in this area are not exposed. As the Roztocze Hills are located in close proximity to the present-day Mid-Polish Anticlinorium, which formed the elevated Łysogóry-Dobrogea Land during the Late Cretaceous, they provide access to various facies, including calcareous sandstones, calcareous mudstones, argillaceous mudstones or clays, various opoka facies.

THE SZOZDY SECTION

The Szozdy section is situated within a railway cutting of the Broad Gauge Metallurgical Railway Line, southwest of Zwierzyniec and close to the small village of Szozdy in southeast Poland (Fig. 3). The fossil assemblage is indicative of a middle Campanian age (Remin et al., 2015a, b; 2022a, b). Notably, plant debris is relatively common, including complete compound leaves in addition to partially carbonized leaves and branches.

The section at Szozdy, together with other sections in the Roztocze Hills (Remin et al., 2022a, b), is easily correlatable with the equivalent interval in the Middle Vistula River Valley composite section (Fig. 4), a reference section for the Upper Cretaceous of the southeastern Polish Basin (e.g., Walaszczyk, 2004; Walaszczyk et al., 2016), and with other sections in south and east Poland (Remin et al., 2022b).

The most prominent feature of the Szozdy section is the presence of tripartite cyclothems (Remin et al., 2022a) typically consisting of three units: calcareous mudstone, calcareous sandstone, and calcareous gaize (Fig. 5), which in this text are generally referred to as mudstone, sandstone, and gaize, respectively. Some cyclothems are incomplete. For instance, cyclothem II lacks the calcareous sandstone unit (Fig. 5).

The total thickness of the Szozdy Delta System cannot be estimated (Remin et al., 2022a, b) since neither the lower nor upper limit of the cyclic succession is known. The exposure at Szozdy (Fig. 3) gives access to ~30–35 metres of the succession over a lateral distance of ~800 m. Other data, such as exposures or well-logs, are not available, precluding any firm conclusions. In the present study, HMAs were collected from a ~12-metre-thick interval (Fig. 5), consisting of six cycles, both complete and incomplete (Fig. 5).

A full description of the Szozdy Delta System lithofacies was provided recently by Remin et al. (2022a), together with facies, bathymetric, and sedimentological characteristics: the reader is referred to this manuscript for further details. As such, only brief descriptions are provided below.

The calcareous mudstone lithofacies (Fig. 3) is dark grey and poorly indurated. The colour is most likely derived from disseminated carbonized organic matter. The clay and silt content is highest present within the cyclothems studied. It was assigned to a prodelta environment (Remin et al., 2022a).

The calcareous sandstone lithofacies (Fig. 3) is yellow to yellow-brownish and poorly indurated. The clay and silt content is ~10% lower than in the underlying calcareous mudstone. The sand fraction, mainly consisting of quartz, is proportionally the highest among the lithofacies recognized in the Szozdy section. The quartz sand is fine-grained overall, though individual grain sizes range up to ~0.25 mm, twice as large as in the underlying calcareous mudstones. It was assigned to a delta lobe environment, relatively close to the river discharge area (Remin et al., 2022a).

The calcareous gaize lithofacies (Fig. 3) is white-grey, fully indurated, and can be extremely hard; in the field, it is expressed as prominent harder beds between more erosion-prone deposits (Fig. 3). This unit contains a limited clay and silt fraction. The $CaCO_3$ content is the highest among the recognized lithofacies (up to 75%). It was assigned to an environment cut off from terrigenous-sourced material, but still in close proximity to land (Remin et al., 2022a).

MATERIAL AND METHODS

Among the 22 samples, 15 from three cyclothems were selected for detailed analysis of heavy minerals; two or three samples from each unit of the cyclothem were collected (Figs. 5 and 8). Samples were mechanically broken into 1–3 cm fragments. To prevent individual grains from being damaged by multiple rounds of hammering, liquid nitrogen disintegration methods were subsequently used, as initially proposed for foraminifera extraction by Remin et al. (2012). In principle, this method ensures that the original grain shapes will be preserved.

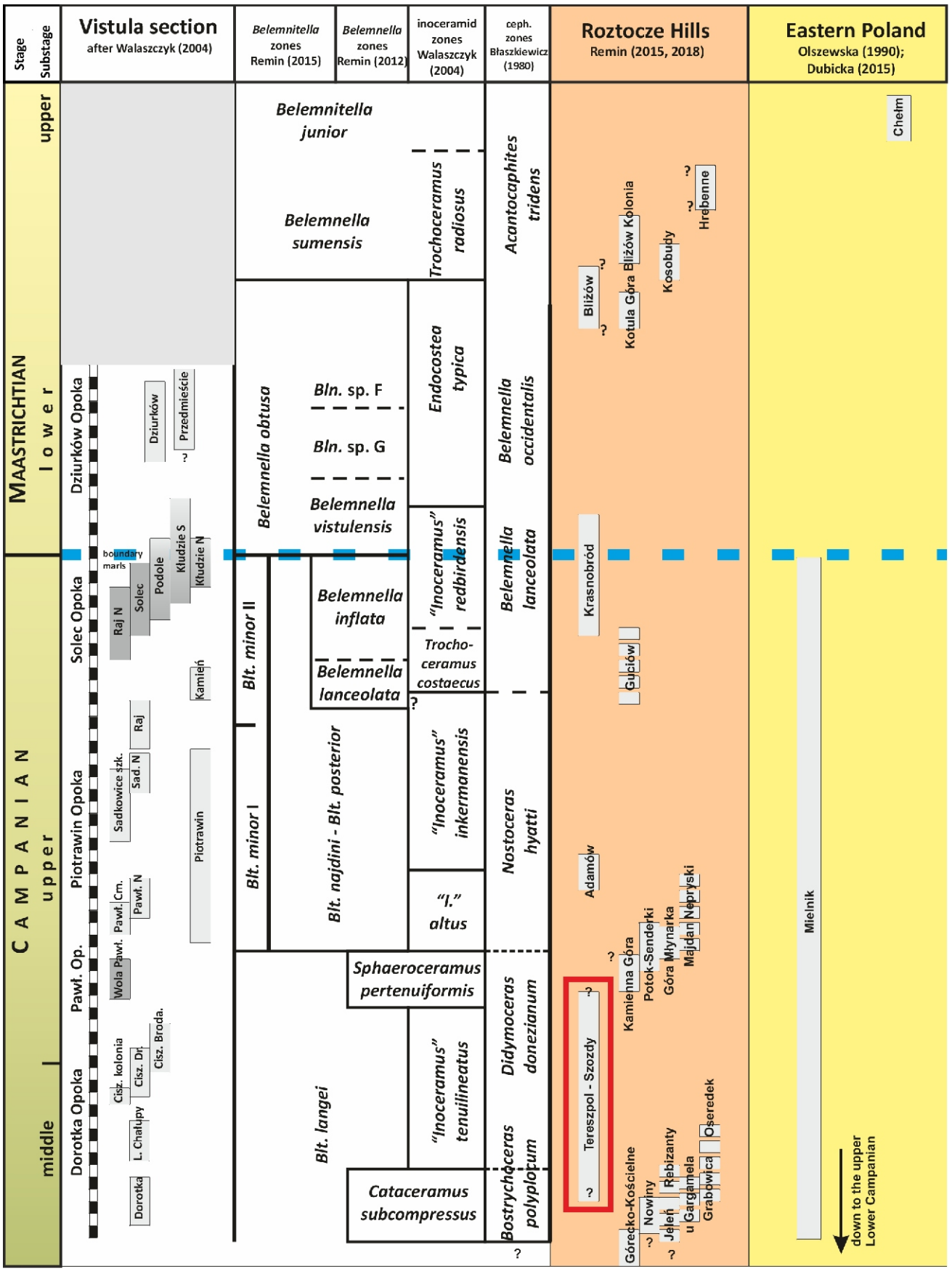

Fig. 4. Stratigraphic position of the Szozdy section (red rectangle marks the known stratigraphic extent of the section) in relation to the Middle Vistula Valley section (left column in white; the metre-scale is valid only for this section; scale bar = 2 m); Roztocze Hills area (middle column in orange); Eastern Poland (right column in yellow)

The biostratigraphic subdivision follows Błaszkiewicz (1980), Walaszczyk (2004), Remin (2012, 2015, 2018), and Remin et al. (2015b, 2022a, b); figure adapted from Remin et al. (2022b). The Campanian/Maastrichtian boundary based on the GSSP Tercis definition (Odin and Laumurelle, 2001) is marked with a blue dashed line (adapted from Remin et al., 2022a, b)

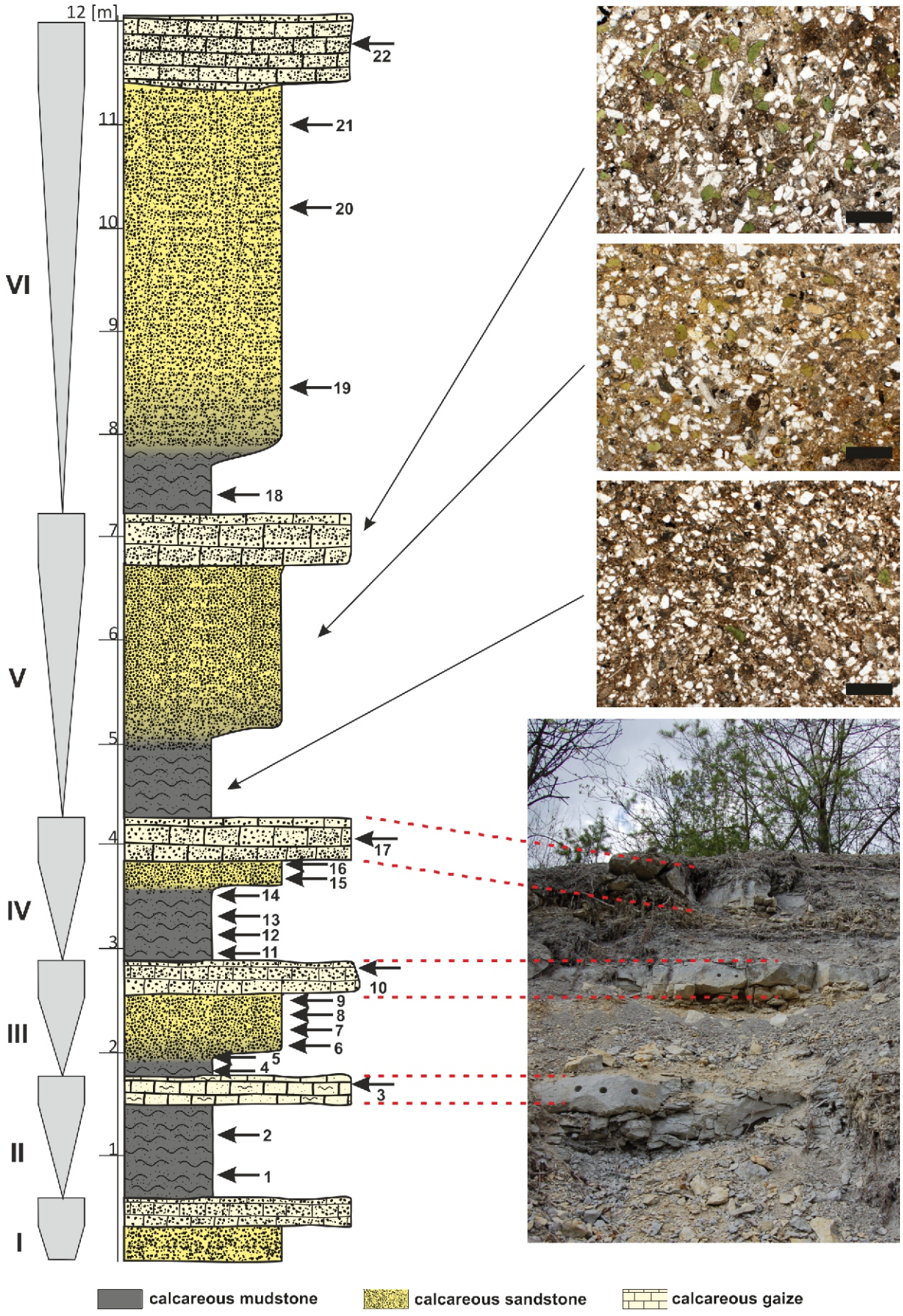

Fig. 5. Lithological column of the Szozdy section (adapted from Remin et al., 2022a)

The left side column (grey) indicates coarsening-upwards cyclothems marked by Roman numerals. Top right: typical thin sections from successive lithofacies of a single cyclothem; scale bar = 500 μm; most white particles represent quartz grains. Bottom right: field photo of a part of the succession with prominent calcareous gaize layers, indicated on the section by red dashed lines. The horizontal scale on the log represents the relative resistance of particular units to weathering. Arrows with numbers indicate the samples collected (adapted from Remin et al., 2022a, b)

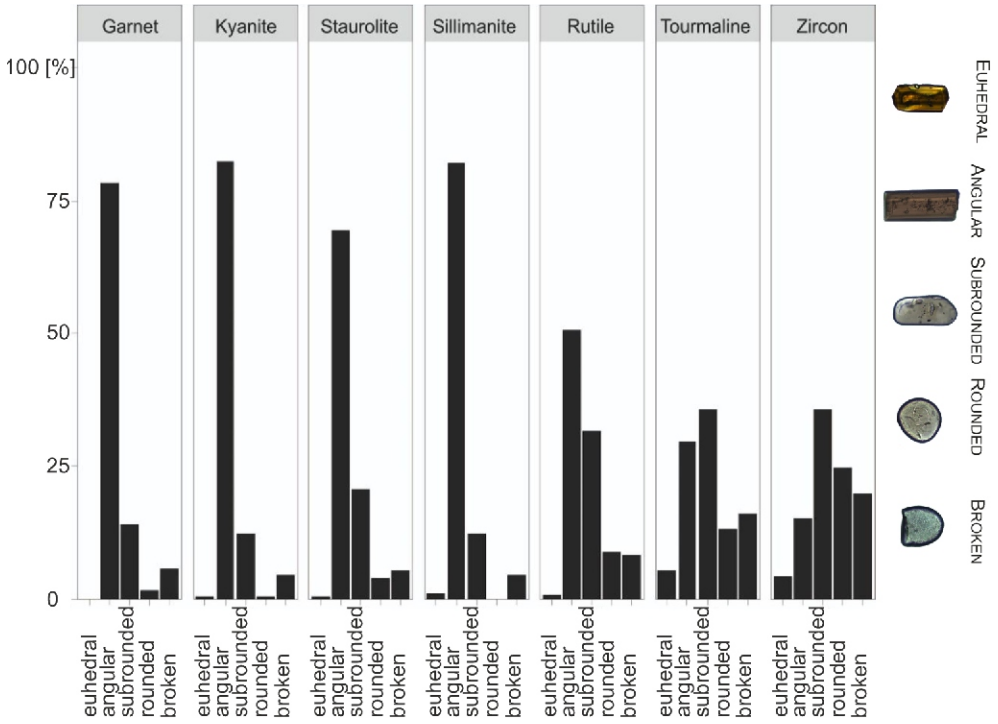

Fig. 6. Degree of roundness of selected mineral phases is exemplified by tourmaline grains from the section studied

The chart depicts the cumulative number of selected mineral grains from all cycles; for details see text

To eliminate carbonate grains, all heavy mineral suites were placed in a 10% acetic acid solution for up to couple of days and further bathed in an ultrasonic cleaner to remove grain coatings, such as clay and Fe-oxides. Acetic acid is commonly used in this type of preparation (apatite does not react with acetic acid) precisely because of the ability of apatite to be preserved in the mineral assemblage in a virtually intact state (see e.g., Mange and Maurer, 1992; Garzanti and Andò, 2007; Garzanti, 2017). Moreover, even the use of heated (70°C) acetic acid does not remove apatite. Subsequently, samples were sieved to obtain the 63–250 μm fraction. Heavy minerals were then separated by centrifuging in sodium polytungstate solution (~3.0 g/cm^3) and recovered by partial freezing with liquid nitrogen. The heavy minerals obtained were immersed in Canada Balsam and examined using a polarizing microscope. At least 200 transparent heavy minerals in each sample were identified. During analysis, a particular focus was placed on the roundness and degree of corrosion (weathering stage) of individual grains; all samples were examined under the same magnification to avoid statistical errors. Additionally SEM was used to examine the micromorphology of selected grains. To check whether a correlation exists between ultrastable ZTR group minerals and garnets, kyanites, and staurolites, Pearson's coefficient was applied (Ryan et al., 2007).

ROUNDNESS

The roundness of the grains examined was classified following the method proposed by Krumbein (1941) and Powers (1953). Five degrees of grain roundness were distinguished: euhedral, angular, subrounded, rounded, and broken (Fig. 6).

DEGREE OF CORROSION

To determine degree of corrosion, the grains analysed were examined using (i) a polarizing microscope with a partially closed diaphragm. Individual grains were subdivided into five groups based on the corrosion of individual grains, following the subdivision proposed by Andò et al. (2012): unweathered, initial, slightly, advanced and final (Fig. 7).

Unweathered minerals contain flat-faced grains with no visible specific chemical weathering structures: for instance, etch pits, mammillary structures, and hacksaw terminations. However, unweathered minerals can possess any shape and may be present in all roundness categories identified.

The surfaces of initially corroded grains are covered by single etch pits with an approximately regular shape formed during chemical weathering. Slightly corroded grain faces show single lenticular pits and a 'sawtooth' form. Etch pits become deeper and longer and start to merge.

Minerals with advanced corroded surfaces are characterized by a combination of expanding etch pits. The etch pits can join perpendicularly or "en échelon", resulting in furrow and groove formation. Grain edges are strongly marked by denticles. Additionally, structures such as mammillary structures are widely developed, especially on garnet and staurolite faces.

Finally corroded grains possess a completely altered outer crystal surface. Bays, grooves and furrows cut the grain surface in any orientation.

HEAVY MINERAL RATIOS

To register changes in petrographic maturity, diagenesis, and/or weathering in pedogenic conditions, or changes in the provenance of terrigenous material and hydrodynamic condi-

Fig. 7. Weathering stages of the heavy minerals analysed are detailed in the text

The column chart on the right side illustrates the cumulative number of grains from all cycles in %. All mineral photos came from the section studied; the scale bars below each mineral represent 100 μm

tions, the following indices were used: the zircon – tourmaline - rutile maturity index (ZTRi) (e.g., Hubert, 1962; Garzanti and Andò, 2007) and the rutile to tourmaline index (RuTidx) (Cyglicki and Remin, 2023). All ratios are based on at least 200 transparent heavy mineral counts in each sample.

TOURMALINE AND GARNET GEOCHEMISTRY

Within individual samples, tourmaline and garnet grains do not show significant variability, i.e. in successive samples similar amounts of similarly pleichroic tourmalines are present; likewise, the range of shapes, colour and weathering structures of garnet grains are similar between samples. As such, chemical composition analysis was only performed for grains from the higher part of the cycle IV (samples 16 and 17; Fig. 5). Most of the garnet and tourmaline grains analysed are homogeneous (unzoned). For this reason, data from them was recalculated using the *WinTac* software of Yavuz et al. (2014). Structural formulae were obtained based on 15 cations (X+Y+Z) to 4 variable anions (V+W, largely consisting of OH+F+Cl) per formula unit. Garnet analyses were recalculated to six end-members (almandine, pyrope, grossular, spessartine, andradite and uvarovite) with the structural formula based on 12 oxygen atoms and 8 cations.

The garnetRF program (Schönig et al., 2021) was used to interpret the results of garnet major element analysis. The program is based on a random forest machine-learning algorithm (Breiman, 2001), and classifies the imported data based on a database of >13,000 garnet major element analyses, with a prediction efficiency close to 90%. The classification scheme allows for the determination of host-rock classes, host-rock composition, and metamorphic facies.

RESULTS

HEAVY MINERAL ASSEMBLAGES – GENERAL CHARACTERISTICS

Heavy mineral assemblages from the Szozdy Delta system are characterized by little variability and a stable composition. The associations analysed include ultrastable phases, such as zircon, tourmaline, and rutile (ZTR), and stable phases like gar-

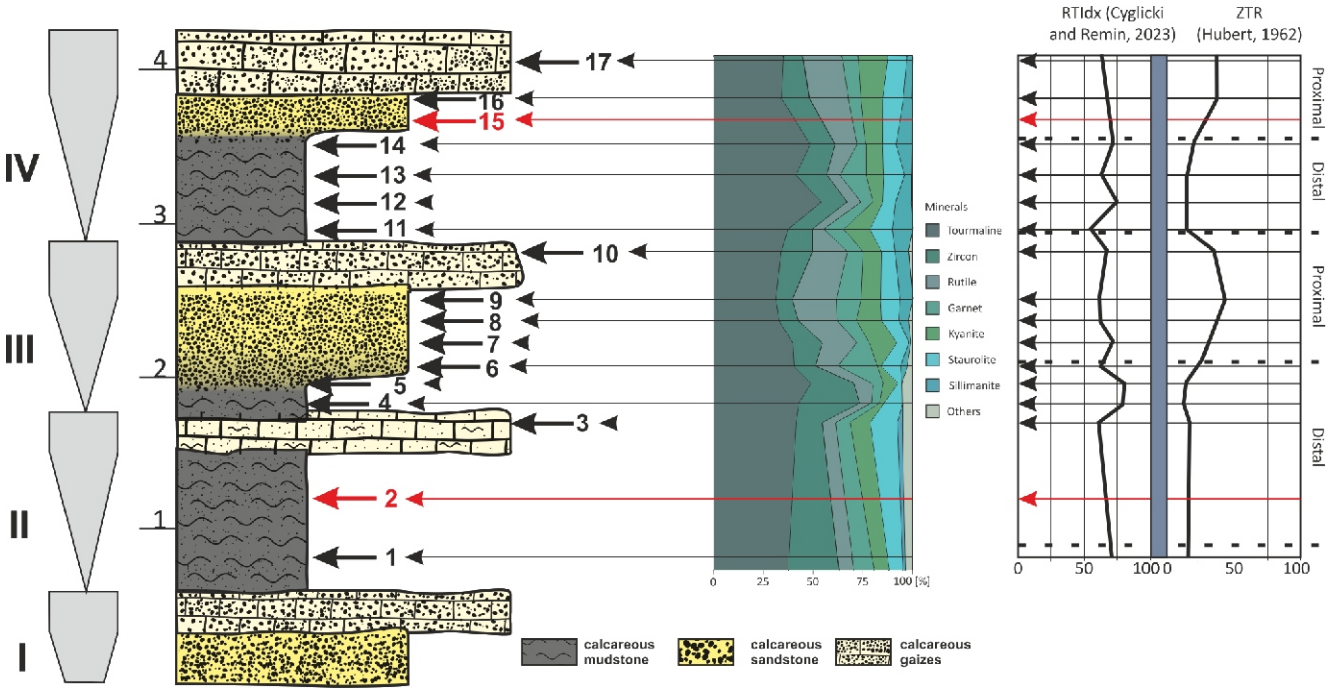

Fig. 8. Litho-weathering log of the Szozdy section (cycles I–IV; first column)

Red arrows indicate samples rich in FeS_2 – in these samples, the heavy minerals cannot be effectively separated. Third column – the percentage abundance of selected mineral phases. Fourth column – values for the ZTR and RuTidx indices are provided along with the interpretation of the sedimentary environment based on RuTidx (according to Cyglicki and Remin, 2023)

net, kyanite, staurolite, and "others" that comprise subordinate species like sillimanite, chlorite, Cr-spinel, epidote and single apatite grains. The mineral assemblages analysed are characterized by the dominance of minerals from the ZTR group and this relates to all units of the cycle, independently of lithofacies.

The most numerous group in the heavy mineral assemblages study are tourmalines. In each sample, they compose at least one-third (31%), and sometimes even half (54%) of the assemblages and their abundance is positively correlated with a particular lithofacies: calcareous mudstone. The average maximum grain length of tourmaline is 150 μm, and their shape is isometric. They were divided into eight pleochroic groups. Brown and green grains dominate. In these groups, most are subrounded and rounded; with ~30–35% angular. A few euhedral grains also are present. In other pleochroic-scheme tourmaline groups, rounded and subrounded grains also prevail. Angular grains account for 15–20%, and broken grains for 18–36% of these populations. Furthermore, euhedral grains are absent. Zoned tourmalines, which constitute ~5–15% of the assemblage, are characterized by blue cores and dark brown overgrowths. They are usually mechanically crushed and angular.

Zircons constitute from 7 to 32% in individual samples, and their abundance is not related to specific lithofacies. The average maximum grain length is 108 μm, and they have an isometric character.

The content of rutile varies between 5–22% and increases in sandy lithofacies. The average grain length of rutile is 120 μm, and their shape is elongated, with a significant disproportion between the longest axis and perpendicular axes x, y. The content of garnets is variable and ranges from 4 to 13%.

Garnet grains are usually colourless and characterized by a high degree of chemical weathering, and their surfaces are clearly sharp-edged. Staurolites are present in samples ranging from 2 to 14%. They are usually yellow, yellow-brown, yellow-orange and pale yellow. Staurolite grains have sharp-edged surfaces and are highly weathered. Kyanite constitutes from 2 to 17% of the samples analysed and are the largest grains, with an average maximum length reaching the limit of the analysed fraction (250 μm). The grains are sharp-edged and heavily corroded, especially along cleavage surfaces. The content of sillimanite in samples ranges from 1 to 10%. Sillimanite grains are sharp-edged and also heavily corroded, but less so compared to kyanite.

ROUNDNESS OF THE HEAVY MINERAL GRAINS ANALYSED

In general, the ZTR mineral grains within the section are mostly subrounded and rounded or broken (>60%; Fig. 6). However, angular crystals are more common in the rutile grains. Relatively few ZTR grains are euhedral (~4%; Fig. 6). Among the garnets, kyanites, and staurolites, angular crystals dominate (~65–80%); oval and rounded crystals are almost entirely absent (Fig. 6).

DEGREE OF CORROSION – SURFACE CHARACTERISTICS OF HEAVY MINERAL GRAINS

The grain surfaces of the ZTR group minerals are characterized by initial to slight corrosion (Fig. 7). Randomly distributed impact and etch pits are among the most commonly observed surface textures. Garnet, kyanite, staurolite and silimanite surfaces show advanced stages of corrosion (Fig. 7).

Sawtooth structures commonly mark the edges of grains. Additionally, mammillary structures, furrows, and grooves are strongly developed, especially on garnet and staurolite faces (cf. Velbel, 1999).

HEAVY MINERAL RATIOS

The ZTR index (Hubert, 1962) ranges between 55 and 80%. The highest ZTR values are associated with the calcareous mudstone lithofacies, which is dominated by tourmaline grains (Fig. 8). The GZi provenance-sensitive index (Morton and Hallsworth, 1994) exhibits values between 10 and 60%.The RuT hydrodynamic index ranges between 12 and 42%, providing insight into the distal and proximal facies (Cyglicki and Remin, 2023).

TOURMALINE GEOCHEMISTRY

Tourmaline is a complex borosilicate with the general formula $XY_3Z_6T_6O_{18}(BO_3)_3V_3W$. The X-site is occupied by Na^+, Ca^{2+}, K^+, Pb^{2+}, Ba^{2+}, Rb^+ or Cs^+, although significant X-site vacancy is also possible. The Y-site forms an octahedral polyhedron that may be occupied by a wide range of multivalent cations: Li^+, Mg^{2+}, Fe^{2+}, Mn^{2+}, Al^{3+}, Cr^{3+}, V^{3+}, Fe^{3+} and Ti^{4+}. The Z-site is occupied by trivalent cations such as Al^{3+}, Fe^{3+}, Cr^{3+}, V^{3+}, although significant Mg^{2+} can be present. The T-site is mainly filled with Si. The V-site chiefly contains an OH^- group and O^{2-}. The W site exclusively contains F^-, with excess O^{2-} and OH^-.

Tourmaline grains (N = 111) from the Szozdy section were analysed using EPMA (Table 1). The analysis showed that most detrital tourmaline grains belong to the alkali-tourmaline primary group, which are enriched in Na^+ and to a lesser extent in K^+ (Fig. 9).

Sodium is the most abundant cation in the X-site, ranging from 0.4 to 0.9 with a mean value of 0.6 apfu (atom per formula unit). X-site vacancy values oscillate from 0.0 to 0.5 (avg. = 0.2 apfu). Calcium abundance in the X-site ranges from 0.0 to 0.5 (avg. = 0.2 apfu).

High X_{Mg} = Mg/(Mg+Fe) ratios (avg. = 0.6) within the alkali group indicates that Mg is the most abundant cation in the Y-site. The Y-site position is occupied by Fe^{2+} (avg. 1.0 apfu), Mg^{2+} (avg. 1.5 apfu), Al^{3+} (avg. 0.25 apfu), Ti^{4+} (avg. 0.09 apfu) and other trace elements such as V^{3+}, Cr^{3+}, Zn^{2+} and Mn^{2+} (avg. <0.01 apfu). Most often, the Z position is fully occupied by Al^{3+}. In some grains, however, the Z position is filled by Mg^{2+} (0.01–0.6 apfu), and subordinately by Cr^{3+} (0.01–0.07 apfu) and V^{3+} (0.01–0.03). The T-position is occupied mostly by Si^{2+}. To a limited extent, the T-position is also occupied by Al^{3+} (avg. 0.7 apfu). More than 75% of the tourmaline grains analysed are dravites (Fig. 10).

GARNET GEOCHEMISTRY

Garnets are among the most important minerals for obtaining information concerning metasomatic, igneous, metamorphic and mantle processes (Baxter et al., 2013; Schönig et al., 2021). Garnets belong to nesosilicates, with the general formula $X_3Z_2(SiO_4)_3$ where: X – Mg, Ca, Fe(II), Mn(II), etc., and Z – Al, Fe(III), Cr(III), V(III), etc. Major-element garnet chemistry depends mainly on temperature, pressure and host-rock composition, and is an excellent tool in sedimentary provenance analysis. In the classical definition, the compositions capture a series of mixed solid solutions among which the following mineral phases occur: almandine $[Fe^{2+}{}_3Al_2(SiO_4)_3]$, pyrope $[Mg_3Al_2(SiO_4)_3]$, spessartine $[Mn^{2+}{}_3Al_2(SiO_4)_3]$, andradite $[Ca_3Fe^{3+}{}_2(SiO_4)_3]$, grossular $[Ca_3Al_2(SiO_4)_3]$, and uvarovite $[Ca_3Cr_2(SiO_4)_3]$.

Garnet grains (N = 50) from the Szozdy section were analysed via EPMA (Table 2). The molar proportions in the garnet from the Szozdy section are constrained within the compositional window: almadine: 50–80 mol%, pyrope: 5–35 mol%, grossular: 2–40 mol%, spessartine: 2–15 mol%. Garnet analyses are usually imperfect (too low or too high; Locock, 2008) but the data we obtained were very close to 100%, sufficient to indicate reliable results.

DISCUSSION

HEAVY MINERAL COMPOSITION VS. PROVENANCE OF DEPOSITS

Most garnet (depends on its composition), in addition to kyanite, staurolite, and sillimanite are generally minerals characteristic of medium-grade metamorphic rocks. However, the parent rocks for ZTR minerals may be either igneous or metamorphic rocks. Furthermore, ZTR group minerals are especially resistant to physical and chemical weathering. High ZTR index values are usually interpreted as reflecting the polycyclic nature of HMAs (Hubert, 1962; Morton and Hallsworth, 1999; Garzanti and Andò, 2019). However, this value can be controlled, *inter alia*, by intense weathering or source rock composition (Garzanti and Andò, 2007; Garzanti, 2017). In our case, the variable tourmaline and rutile proportions in successive samples of the section are a result of the hydrodynamics of the depositional environment during the formation of successive units of the cycle (Remin et al., 2022a; Cyglicki and Remin, 2023).

A positive correlation between two minerals may arise for several reasons. Firstly, it could be due to both minerals originating from the same source. In such cases, positive correlations will occur along strike and at all stratigraphic levels where materials from that source are present. Secondly, the two mineral species may come from different sources whose importance is increasing or decreasing simultaneously at a particular location and time. If the influence of both sources is not consistent throughout the extent and life of a basin, the positive correlations will not be repeated along the strike or at different stratigraphic levels (Ryan et al., 2007). Negative correlation may arise as a consequence of cutting off one source with the simultaneous amplification of another source. As a result, minerals typical for the active source region would be present in excess relative to mineral phases coming from the inactive source. An additional driver of negative correlations may be through geochemical processes that selectively remove labile minerals, for instance during weathering (cf. Ryan et al., 2007).

As exemplified in Figure 8, as the proportion of ultrastable ZTR minerals increased, the proportion of garnets, kyanites and staurolites decreased. As suggested above, the moderate negative correlation of garnets, kyanites and staurolites to ZTR (–0.60, –0.65 and –0.78 respectively) might be interpreted as a result of the selective removal of susceptible mineral phases by weathering and/or hydrodynamic sorting (e.g., Cyglicki and Remin, 2023), especially for garnets and staurolites, and/or mechanical abrasion during multiple recycling phases, e.g. for kyanites (Figs. 6–8; Freise, 1931; Thiel, 1940, 1945; Dietz, 1973).

Table 1

Representative microprobe analyses of the tourmaline grains analysed from the Szozdy section

	grain 1	grain 2	grain 3	grain 4	grain 5	grain 6	grain 7	grain 8	grain 9	grain 10	grain 11	grain 12
SiO_2	36.611	36.38	35.81	36.03	36.27	36.55	34.81	35.96	35.75	35.92	35.79	36.32
TiO_2	0.49	0.47	1.06	0.26	0.38	0.69	1.5	0.89	0.53	0.85	0.79	0.63
Al_2O_3	31.1	31.53	29.44	33.7	35.47	32.52	33.19	27.99	32.2	33.44	28.92	31.07
V_2O_3	0.14	0	0.06	0	0.03	0.09	0.02	0.07	0	0	0.1	0
Cr_2O_3	0	0	0	0	0.11	0	0	0.03	0.07	0	0.11	0.03
MgO	6.61	7.72	6.17	2.69	5.38	7.82	4.31	8.18	0.47	5.51	6.76	6.07
MnO	0.05	0	0	0.46	0.11	0	0.04	0.03	0.27	0	0.09	0.02
CaO	1.16	1.31	0.61	0.34	0.49	0.95	0.79	2.37	0.07	0.83	0.82	0.49
Na_2O	1.75	1.84	2.13	1.95	1.51	2.03	1.68	1.41	2.62	1.61	2.19	2.31
K_2O	0.01	0.02	0.01	0.05	0.05	0	0.03	0.06	0.05	0.04	0	0.04
F	0.17	0	0.16	0	0.16	0.16	0.16	0.17	1.02	0	0	0.16
B_2O_3*	10.48	10.51	10.12	10.4	10.62	10.61	10.3	10.38	10.03	10.42	10.31	10.41
H_2O	3.33	3.47	3.26	3.32	3.2	3.41	3.21	3.41	2.89	3.31	3.44	3.38
O=F	0.07	0	0.07	0	0.07	0.07	0.07	0.07	0.43	0	0	0.07
Total	99.98	99.56	96.84	100.4	99.74	100.1	98.72	100	99.23	98.83	99.12	99.65
T-site												
Si^{4+}	6.07	6.02	6.15	6.03	5.94	5.99	5.88	6.02	6.2	5.99	6.03	6.06
Al^{3+}	0	0	0	0	0.06	0.01	0.12	0	0	0.01	0	0
Subtotal	6.07	6.02	6.15	6.03	6	6	6	6.02	6.2	6	6.03	6.06
Y, Z-site-sites												
Al^{3+}	6.08	6.15	5.96	6.64	6.78	6.26	6.48	5.53	6.58	6.56	5.75	6.11
Ti^{4+}	0.06	0.06	0.14	0.03	0.05	0.08	0.19	0.11	0.07	0.11	0.1	0.08
Cr^{3+}	0	0	0	0	0.01	0	0	0	0.01	0	0.01	0
V^{3+}	0.02	0	0.01	0	0	0.01	0	0.01	0	0	0.01	0
Fe^{2+}	1.11	0.88	1.15	1.56	0.82	0.73	1.24	1.28	1.98	0.96	1.36	1.23
Mn^{2+}	0.01	0	0	0.07	0.02	0	0.01	0	0.04	0	0.01	0
Mg^{2+}	1.64	1.9	1.55	0.67	1.31	1.91	1.09	1.58	0.12	1.37	1.47	1.51
Subtotal	8.93	8.98	8.85	8.98	9	9	9	8.98	8.8	9	8.97	8.94
X-site												
Ca^{2+}	0.21	0.23	0.11	0.06	0.09	0.17	0.14	0.43	0.01	0.15	0.15	0.09
Na^{+}	0.56	0.59	0.71	0.63	0.48	0.65	0.55	0.46	0.88	0.52	0.72	0.75
K^{+}	0	0	0	0.01	0.01	0	0.01	0.01	0.01	0.01	0	0.01
vacancy	0.23	0.18	0.18	0.3	0.42	0.19	0.3	0.11	0.1	0.32	0.14	0.16
Subtotal	1	1	1	1	1	1	1	1	1	1	1	1
OH^{-}	3.68	3.82	3.74	3.7	3.49	3.73	3.61	3.81	3.35	3.68	3.86	3.76
F^{-}	0.09	0	0.09	0	0.08	0.08	0.09	0.09	0.56	0	0	0.08
Subtotal	3.77	3.82	3.82	3.7	3.58	3.81	3.7	3.9	3.9	3.68	3.86	3.84
Mg/(Mg+Fe)	0.6	0.69	0.58	0.3	0.62	0.72	0.47	0.55	0.06	0.59	0.52	0.55
Mineral	Dravite	Dravite	Dravite	Schorl	Dravite	Dravite	Schorl	Dravite	Fluor-schorl	Dravite	Dravite	Dravite

* Calculated on the basis of ideal stoichiometry (B = 3 apfu; OH + F + Cl = 4 apfu); 0 means below detection limit

ROUNDNESS OF HEAVY MINERALS VS. PROVENANCE OF DEPOSITS

The kyanite grains are almost exclusively angular, with clearly visible cleavage. Angular garnet and staurolite shapes were emphasized by strongly advanced weathering (selective leaching in soil); subrounded and rounded grains occur subordinately. High values of the ZTR index and domination of well-rounded crystals of zircon, tourmaline and rutile (Fig. 6) might indicate possible sedimentary or metasedimentary origin (compare the tourmaline geochemistry results).

Additionally, the rounded shape of most tourmalines suggests they most probably passed through more than one sedimentation-diastrophic cycle. On the other hand, the minor presence of euhedral tourmalines may be indicative of another source area composed of freshly weathered rocks. However, it is also possible that idiomorphic tourmaline crystals were created by the progressive metamorphism of sedimentary rocks (Sperlich et al., 1996; Henry and Dutrow, 2012). This hypothesis is supported by the presence of regenerated tourmaline grains that rebuilt their idiomorphic shape on formerly round

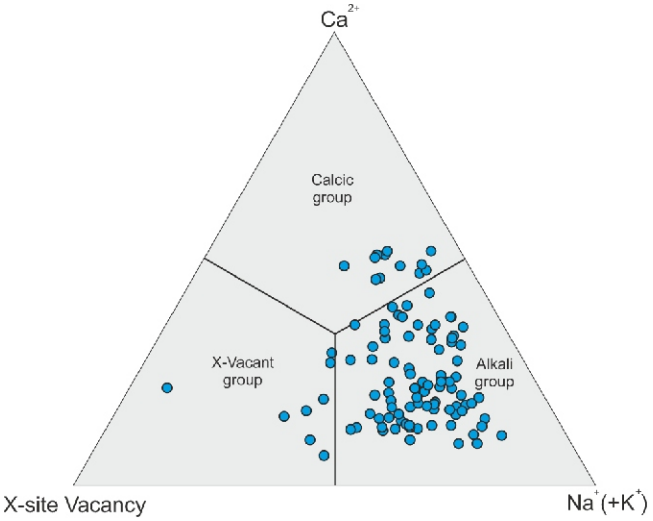

Fig. 9. Chemical composition of detrital tourmalines in the X-site vacancy – Na + K – Ca ternary diagram (Yavuz et al., 2014)

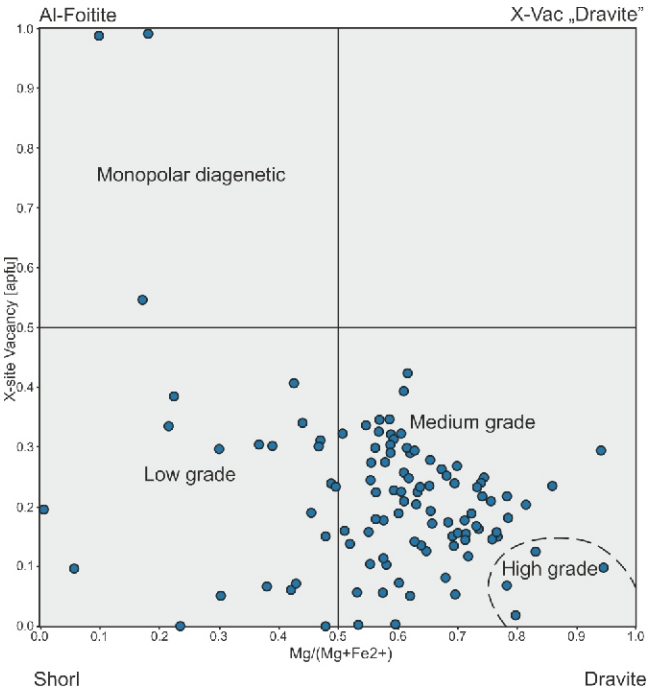

Fig. 10. X-site vacancy vs. X_{Mg} for tourmaline from the Szozdy section

The dashed line and boxes for Al-poor metapelites are based on Henry and Dutrow (1996)

tourmaline detrital cores under upper greenschist to amphibolite facies conditions (Sperlich et al., 1996). This interpretation would also explain why euhedral crystals are present almost exclusively in the tourmaline group.

TOURMALINE GEOCHEMISTRY VS. PROVENANCE OF DEPOSITS

In all the samples studied, homogeneous tourmaline grains dominate; however, the contribution of zoned tourmalines with visible overgrowths can reach 15%. Zoned grains possess a detrital core indicative of the parent rock, whereas overgrowths are the response to changes in P-T conditions in the metamorphic zone (Henry and Dutrow, 1992). In most cases, there are sharp chemical discontinuities between the detrital core and the overgrowths (Fig. 11). Overgrowths can be divided into internal and outer rims. Inner rims develop asymmetrically towards the antilogous pole (+) (Fig. 11). They originate in diagenetic or low greenschist facies conditions (stage I; Fig. 11). As a result of progressive metamorphism, (upper greenschist and amphibolites facies), outer rims develop, in parallel directions towards

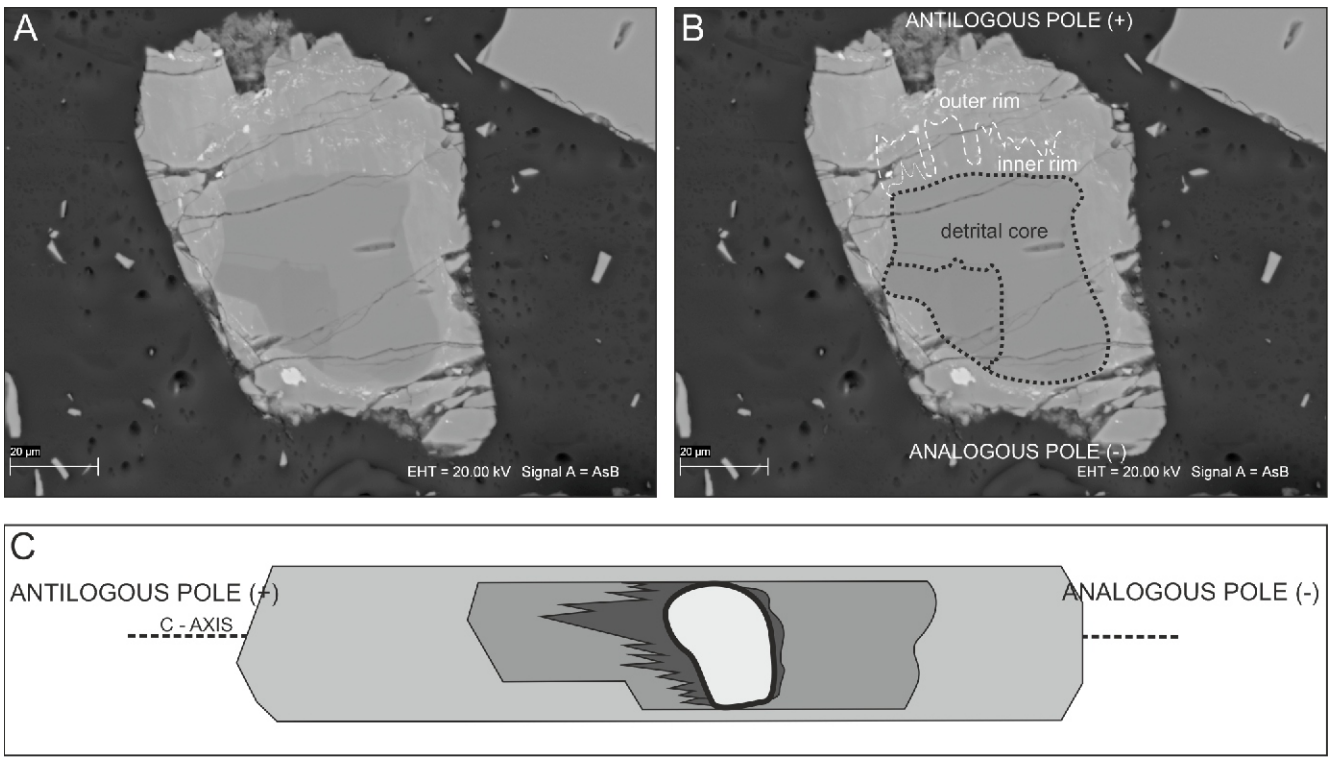

Fig. 11A – back-scattered electron (BSE) image of asymmetrically overgrown detrital tourmaline from the Szozdy section; B – annotated image (compare image A) with interpretation; C – example of detrital tourmaline core with three metamorphic overgrowth zones (based on Sperlich et al., 1996)

Table 2

Representative microprobe analyses of the garnet grains analysed from the Szozdy section

Analysis (wt.%)	grain 1	grain 2	grain 3	grain 4	grai 5	grain 6	grain 7	grain 8	grain 9	grain 10	grain 11	grain 12
SiO_2	37.007	37.213	37.333	37.100	36.656	36.022	37.630	37.501	36.899	37.942	37.942	37.662
TiO_2	0.061	0.071	0.020	0.000	0.035	0.034	0.032	0.139	0.010	0.098	0.029	0.094
Al_2O_3	21.284	21.132	21.238	21.266	20.983	20.673	21.734	21.342	21.228	21.213	21.343	21.460
Cr_2O_3	0.028	0.018	0.017	0.000	0.012	0.000	0.013	0.000	0.011	0.040	0.005	0.000
FeO/ FeO_{tot}	29.562	30.823	35.865	35.935	36.594	30.992	29.557	26.763	34.478	26.222	27.963	28.252
MnO	6.429	2.539	1.068	1.356	2.535	9.563	4.036	2.010	1.275	1.409	0.501	0.727
MgO	2.527	2.822	2.487	2.828	1.949	1.106	5.689	2.402	3.370	4.558	3.022	3.110
CaO	2.877	5.350	1.917	1.915	0.706	0.740	1.163	9.520	2.174	7.938	9.039	8.287
Na_2O	0.073	0.048	0.000	0.056	0.023	0.000	0.006	0.046	0.051	0.032	0.000	0.000
Total (calc)	99.848	100.016	99.945	100.456	99.493	99.130	99.860	99.723	99.496	99.452	99.844	99.592
Recalc (wt.%)												
final FeO	29.27	29.88	35.87	35.23	36.59	30.5	29.28	26.24	33.81	25.59	27.92	28.22
final Fe_2O_3	0.33	1.05	0	0.78	0	0.55	0.31	0.58	0.74	0.71	0.05	0.03
final MnO	6.43	2.54	1.07	1.36	2.54	9.56	4.04	2.01	1.28	1.41	0.5	0.73
final Mn_2O_3	0	0	0	0	0	0	0	0	0	0	0	0
Total	99.887	100.124	99.952	100.535	99.494	99.185	99.897	99.78	99.573	99.531	99.85	99.593
End-members												
Henritermierite	0.00%	0.00%	0.00%	0.00%	0.00%	0.00%	0.00%	0.00%	0.00%	0.00%	0.00%	0.00%
Blythite	0.00%	0.00%	0.00%	0.00%	0.00%	0.00%	0.00%	0.00%	0.00%	0.00%	0.00%	0.00%
Katoite	0.00%	0.00%	0.00%	0.00%	0.00%	0.00%	0.00%	0.00%	0.00%	0.00%	0.00%	0.00%
FCa garnet	0.00%	0.00%	0.00%	0.00%	0.00%	0.00%	0.00%	0.00%	0.00%	0.00%	0.00%	0.00%
FMn garnet	0.00%	0.00%	0.00%	0.00%	0.00%	0.00%	0.00%	0.00%	0.00%	0.00%	0.00%	0.00%
Yttrogarnet	0.00%	0.00%	0.00%	0.00%	0.00%	0.00%	0.00%	0.00%	0.00%	0.00%	0.00%	0.00%
Kimzeyite	0.00%	0.00%	0.00%	0.00%	0.00%	0.00%	0.00%	0.00%	0.00%	0.00%	0.00%	0.00%
Kimzeyite-Fe	0.00%	0.00%	0.00%	0.00%	0.00%	0.00%	0.00%	0.00%	0.00%	0.00%	0.00%	0.00%
Tin garnet	0.00%	0.00%	0.00%	0.00%	0.00%	0.00%	0.00%	0.00%	0.00%	0.00%	0.00%	0.00%
Schorlomite	0.00%	0.00%	0.00%	0.00%	0.00%	0.00%	0.00%	0.00%	0.00%	0.00%	0.00%	0.00%
Schorlomite-Al	0.18%	0.21%	0.00%	0.00%	0.11%	0.11%	0.10%	0.42%	0.03%	0.29%	0.00%	0.28%
Morimotoite	0.00%	0.00%	0.00%	0.00%	0.00%	0.00%	0.00%	0.00%	0.00%	0.00%	0.17%	0.00%
NaTi garnet	0.00%	0.00%	0.00%	0.00%	0.00%	0.00%	0.00%	0.00%	0.00%	0.00%	0.00%	0.00%
Morimotoite-Mg	0.00%	0.00%	0.00%	0.00%	0.00%	0.00%	0.00%	0.00%	0.00%	0.00%	0.00%	0.00%
Morimotoite-Fe	0.00%	0.00%	0.00%	0.00%	0.00%	0.00%	0.00%	0.00%	0.00%	0.00%	0.00%	0.00%
Majorite	0.00%	0.00%	0.00%	0.00%	0.00%	0.00%	0.00%	0.00%	0.00%	0.00%	0.17%	0.00%
Sc garnet	0.00%	0.00%	0.00%	0.00%	0.00%	0.00%	0.00%	0.00%	0.00%	0.00%	0.00%	0.00%
Goldmanite	0.00%	0.00%	0.00%	0.00%	0.00%	0.00%	0.00%	0.00%	0.00%	0.00%	0.00%	0.00%
Yamatoite	0.00%	0.00%	0.00%	0.00%	0.00%	0.00%	0.00%	0.00%	0.00%	0.00%	0.00%	0.00%
Uvarovite	0.09%	0.06%	0.05%	0.00%	0.04%	0.00%	0.04%	0.00%	0.04%	0.12%	0.02%	0.00%
Knorringite	0.00%	0.00%	0.00%	0.00%	0.00%	0.00%	0.00%	0.00%	0.00%	0.00%	0.00%	0.00%
Spessartine	14.62%	5.73%	2.44%	3.07%	5.85%	22.30%	9.01%	4.51%	2.90%	3.13%	1.12%	1.63%
Pyrope	10.11%	11.20%	9.98%	11.27%	7.92%	4.54%	22.36%	9.48%	13.49%	17.85%	11.66%	12.27%
Almandine	65.71%	66.54%	80.75%	78.78%	83.38%	70.21%	64.55%	58.10%	75.93%	56.20%	61.52%	62.45%
Grossular	8.00%	14.64%	5.48%	5.49%	1.91%	2.08%	3.15%	26.59%	6.19%	20.79%	25.21%	23.21%
Andradite	0.00%	0.36%	0.00%	0.00%	0.00%	0.00%	0.00%	0.00%	0.00%	1.13%	0.14%	0.00%
Calderite	0.00%	0.00%	0.00%	0.00%	0.00%	0.00%	0.00%	0.00%	0.00%	0.00%	0.00%	0.00%
Skiagite	0.00%	0.00%	0.00%	0.00%	0.00%	0.00%	0.00%	0.00%	0.00%	0.00%	0.00%	0.00%
Khoharite	0.00%	0.00%	0.00%	0.00%	0.00%	0.00%	0.00%	0.00%	0.00%	0.00%	0.00%	0.00%
Remainder	1.28%	1.26%	1.30%	1.39%	0.79%	0.77%	0.80%	0.90%	1.42%	0.48%	0.00%	0.16%
Total	99.99%	100.00%	100.00%	100.00%	100.00%	100.01%	100.01%	100.00%	100.00%	99.99%	100.01%	100.00%
Quality Index	Excellent	Excellent	Fair	Excellent	Excellent	Superior	Superior	Superior	Excellent	Superior	Superior	Superior

0 means below detection limit

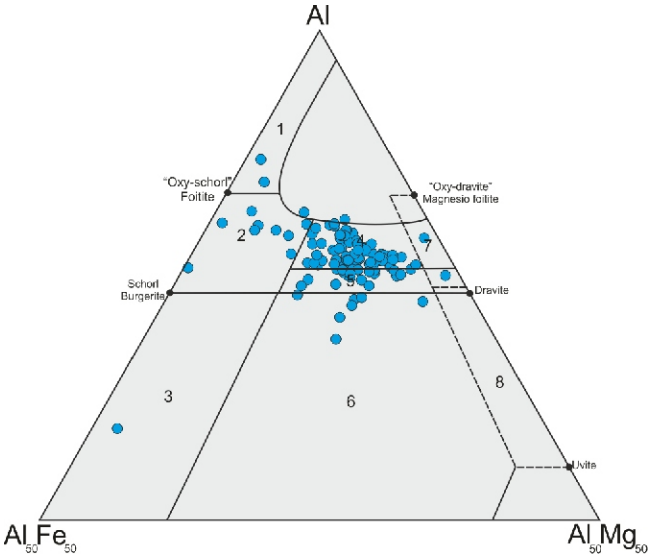

Fig. 12. Al–Fe(tot)$_{50}$–Mg$_{50}$ ternary diagrams for tourmaline from various lithologies (after Henry and Guidotti, 1985)

1 – Li-rich granitoid pegmatites and aplites; 2 – Li-poor granitoids and their associated pegmatites and aplites; 3 – ferric iron-rich quartz-tourmaline rocks (hydrothermally altered granites); 4 – metapelites and metapsammites coexisting with an Al-saturated phase; 5 – metapelites and metapsammites not coexisting with an Al-saturated phase; 6 – ferric iron-rich quartz-tourmaline rocks, calc-silicate rocks, and metapelites; 7 – low-Ca metaultramafics and Cr, V-rich metasedimentary rocks; 8 – metacarbonates and meta-pyroxenites. Blue dots indicate tourmaline geochemistry from the Szozdy section

antilogous and analogous poles (stages II and III; Fig. 11). In the amphibolitic facies, full regeneration of tourmaline grains occurs (Sperlich et al., 1996).

In the grains studied, the inner and outer rims develop asymmetrically towards the antilogous poles (Fig. 11C), which suggests their formation under low-grade metamorphism (Krynine, 1946; Henry and Dutrow, 1992, 1996, 2012).

In Henry's and Guidotti's (1985) ternary diagram (Fig. 12), the vast majority of tourmalines examined in this study occupy fields 4 and 5, characteristic of metamorphosed sedimentary rocks. Of these, most occupy field 4, corresponding to rocks rich in an aluminum phase such as kyanite and staurolite that co-create these mineral patterns. Some grains correspond to tourmalines derived from Li-poor granitoids and their vein counterparts (Fig. 12; field 2). A potential source of two tourmaline grains may be ultramafic rocks and metasedimentary rocks enriched in Cr and V (Fig. 12; field 7), which additionally supports the presence of Cr-spinels. The chemical composition of the detrital cores indicates that they formed in igneous conditions (Fig. 12; field 2 granitoids), while overgrowths are associated with metasedimentary rocks (Fig. 12; field 4).

Analysis of Ca, Ti, and F contents enables the division of the rock types into several subtypes (Table 3; Henry and Dutrow, 1992). Most tourmalines (44%) represent type 1 Al-rich metapelites. Such tourmalines are characterized by low to medium Ca (0.00–0.25 apfu), Ti (0.00–0.20 apfu), and F (0.00–0.30 apfu) concentrations and a strictly defined composition shown on a Al-Fe-Mg ternary diagram (Henry and Dutrow, 1992). These features are consistent with tourmalines from metapelites in equilibrium with aluminous minerals such as staurolite or kyanite (Henry and Guidotti, 1985), which aligns well with the mineral association recognised in the Szozdy section. 20% of the grains correspond to type 2 Al-rich metapelites (Table 3), and are characterized by increased Al, Mg, and Ca content (0.10–0.45 apfu). Grains with such compositions are most likely derived from a metamorphosed aluminous marl (Povondra and Novak, 1986). Type 1 Al-poor metapelites (Table 3) are represented by 12% tourmaline grains with a moderate X_{Mg} range (= 0.5 to 0.6), relatively low Ca content (0.00–0.10 apfu). and low to medium Ti (~0.15 apfu), and F (0.00–0.10 apfu) content. These compositions are of tourmalines derived from phyllite or metasiltstone (Henry and Dutrow, 1992).

Several tourmaline grains might have been derived from low-Li granitoid plutons or Li-enriched pegmatites (Type 1 and 2 granitoids; Fig. 12 and Table 3). By comparison with type 1 granitoids, type 3 granitoids (Table 3) are enriched in Fe and F (Henry and Dutrow, 1992); this composition is mainly characteristic of the detrital cores of zonal tourmalines. The remaining tourmalines represent type 1 and 2 Fe^{3+}-rich quartz tourmaline rocks (Fig. 12 and Table 3), most likely hydrothermally altered (Jones et al., 1981).

Many tourmalines from the Szozdy section are derived from low to medium-grade metapelitic rocks, based on their F and Mg contents (Fig. 13). A few grains show igneous provenance (Fig. 13). Metapelite tourmalines are characterized by Mg ranging from 1.25 to 2.25 apfu and F below 0.5 apfu (Fig. 13). Tourmalines from igneous rocks are generally characterized by an elbaite/shorl composition (Fig. 13). Those from Li-rich granitoids tend to have a higher F content in comparison to

Table 3

Possible source rock types for the detrital tourmaline components

Ca	Ti	F	Al-Fe-Mg field	Possible source rock type	Percent of grains
+/–	+/–	+/–	4	Type 1 Al-rich metapelites	44
+	+/–	+/–	4	Type 2 Al-rich metapelites	20
–	–	–	5	Type 1 Al-poor metapelites	12
+/–	+/–	+/–	2	Type 1 Granitoid	7
–	+	–	5	Type 2 Al-poor metapelites	6
+/–	+/–	+	2	Type 3 Granitoid	4
+	+	–	6	Type 1 Fe^{3+}-rich quartz-tourmaline rocks	5
–	–	–	6	Type 2 Fe^{3+}-rich quartz-tourmaline rocks	2

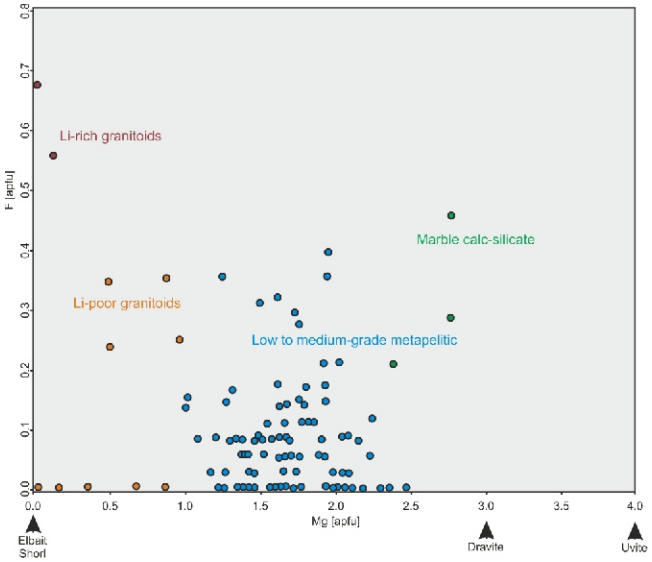

Fig. 13. Fluorine and magnesium concentrations characteristic of igneous and metamorphic tourmalines from the Szozdy section (based on Henry and Dutrow, 1996)

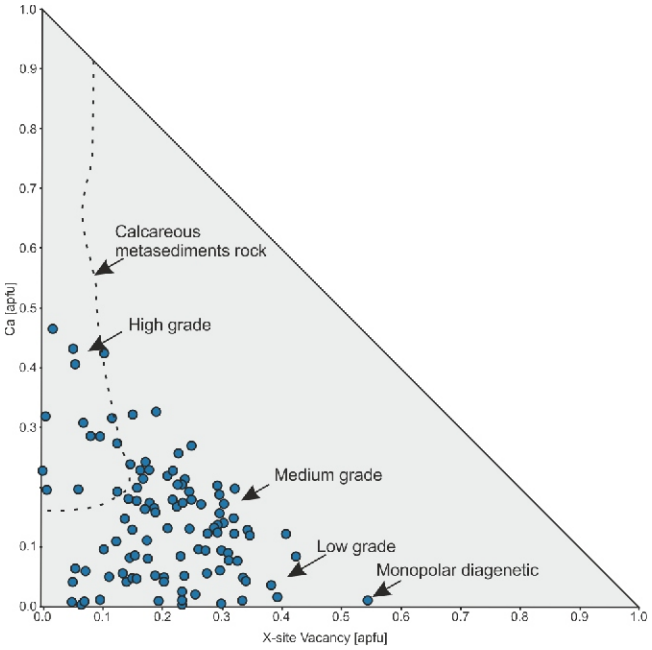

Fig. 14. Ca vs. X-Site vacancy systematics for tourmalines from the Szozdy section (based on Henry and Dutrow, 1996)

those from Li-poor granitoids (Fig. 13). Marble and calc-silicate tourmalines show a relatively high proportion of F, with a general tendency to shift the composition towards uvite (Fig. 13).

Most tourmalines from the Szozdy section come from medium-grade metapelitic rocks (Figs. 12–14). They are characterized by a mean total Al content of 6.19 apfu, of which tetrahedral and octahedral Al constitute 0.07 and 0.25 apfu, respectively. The X-site vacancy is, on average, 0.22 apfu.

The progressive increase in tetrahedral Al from values close to 0 to 0.15 apfu is associated with a progressive increase in host-rock metamorphism from low- to high-grade. At the same time, the X-site vacancy is reduced from 0.55 apfu to nearly 0 apfu, which is associated with an increase in temperature to ~750°C (Fig. 14; Henry and Dutrow, 1996).

GARNET GEOCHEMISTRY

Using the classic approach, the EPMA analysis (Table 2) allowed us to compositionally divide garnet grains into four genetic types (Mange and Morton, 2007; Meres, 2008; Aubrecht et al., 2009): almandine, pyrope, spessartine, and grossular.

The garnets from the Szozdy section can be further subdivided into four groups that differ in their chemical compositions (Fig. 15). The first and largest group consists of grains with higher almandine (60–70%), lower pyrope (20–35%), and low spessartine (<2%) and grossular (<5%) contents. The second group consists of grains with almandine composition >70%, pyrope <20%, spessartine 2–10%, and grossular <7%. The third group is characterized by increased grossular content (~30%) and reduced almandine content (50-60%). The fourth group, in relation to the previous three, is distinguished by increased spessartine content (>8%).

Based on the ternary diagrams of Meres (2008), most garnet grains from the Szozdy section occupy fields C1 and C2 (Fig. 15A, B). The C-fields correspond to garnets created in amphibolite facies conditions (Fig. 15A, B), with C1 characteristic of the transitional subgroup between granulite and amphibolite facies conditions and the C2 subgroup usually linked to amphibolite facies conditions *sensu stricto* (Meres, 2008; Aubrecht et al., 2009). Six grains occupy field B (Fig. 15A, B), which corresponds to garnets from eclogite and granulite facies conditions. Importantly, this classification scheme does not show garnets typical of high-pressure/ultra-high-pressure conditions.

Using the classification of Mange and Morton (2007) the garnets from the Szozdy section can be subdivided into four metamorphic origins: type A – high grade (granulite facies) metasedimentary rocks; type Bii – low grade (amphibolite facies) metasedimentary rocks; Type Bi – intermediate-acidic igneous rock, enriched in Mn and containing <10% Ca; and Type Ci – metamorphic mafic rocks, such as mafic gneisses (Fig. 5C). The overall picture of grain type distribution may be distorted due to their different susceptibility to weathering. Generally, garnet types Bii and C are less stable than types A and Bi.

As interpreted from garnetRF, the host rock for the garnet grains under analysis was primarily metamorphic (Schönig et al., 2021). However, garnets derived from igneous rock constitute a minor proportion of the overall assemblage (Fig. 16A, D). The host-rock composition primarily corresponds to intermediate felsic rock (Fig. 16B, D). The metamorphic rocks were mainly affected by pressure-temperature conditions corresponding to amphibolite facies (Fig. 16C, D). Conditions suitable for amphibolite facies are corroborated by the presence of kyanite, staurolite (Fig. 17) and co-occurring dravites (Fig. 12) which coexist under the temperature and pressure conditions of 500–700°C and 0.6–0.8 GPa. Further corroboration takes the form of regenerated tourmaline grains, that were rebuilt on old detrital cores. According to this classification, some grains were subjected to P-T conditions corresponding to granulite facies.

Since most of the garnets were formed under amphibolite/greenschist conditions, as indicated by classical interpretations, the results obtained from garnetRF analyses (Schönig et al, 2021) show additionally the presence of a few grains that might originated under blueschist and/or eclogite facies condi-

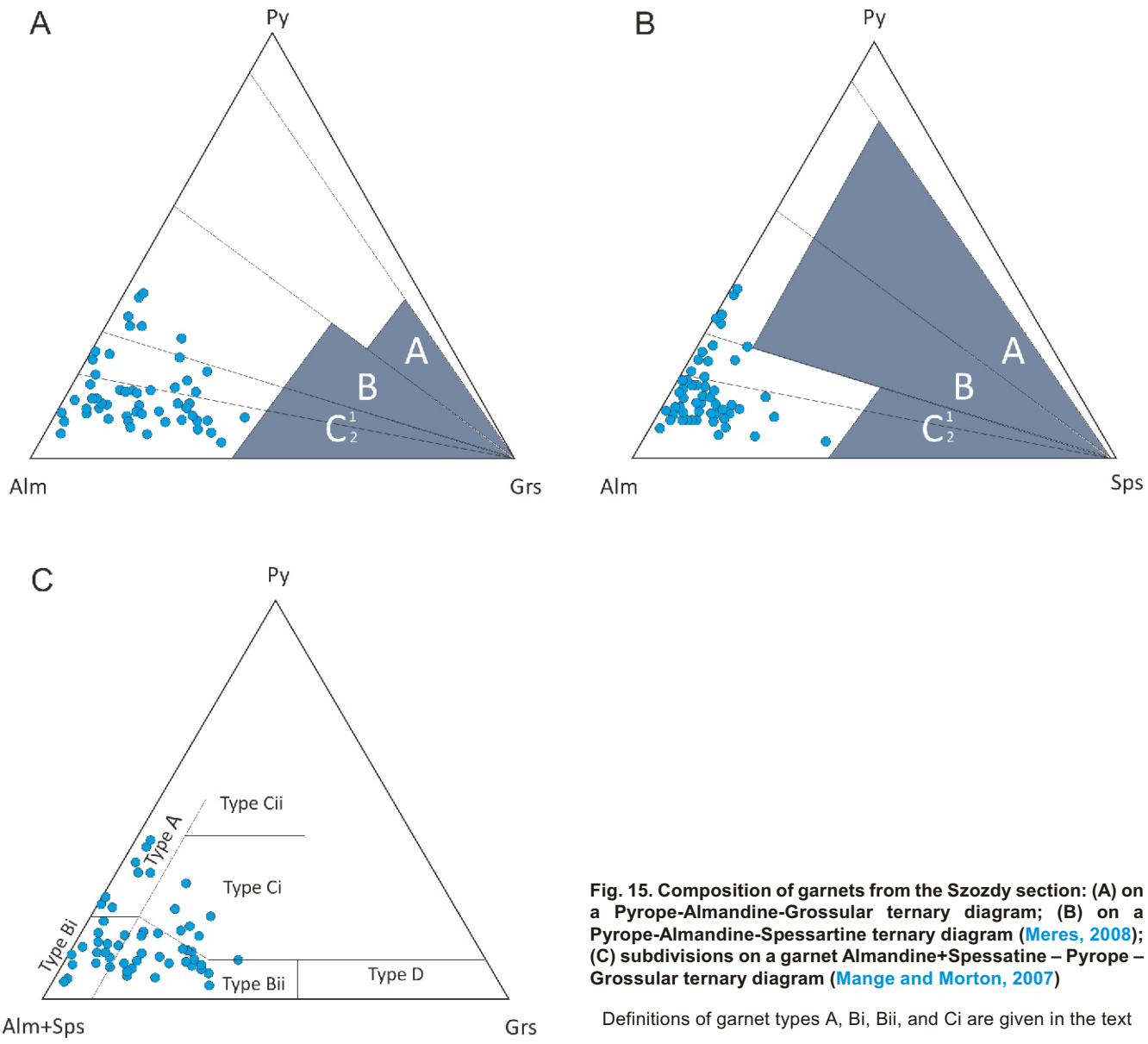

Fig. 15. Composition of garnets from the Szozdy section: (A) on a Pyrope-Almandine-Grossular ternary diagram; (B) on a Pyrope-Almandine-Spessartine ternary diagram (Meres, 2008); (C) subdivisions on a garnet Almandine+Spessatine – Pyrope – Grossular ternary diagram (Mange and Morton, 2007)

Definitions of garnet types A, Bi, Bii, and Ci are given in the text

tions. Although such an interpretation is highly speculative, since only few such grains were found, it is however consistent with the results from tourmaline: that is, grains derived from Al-poor metapelitic rocks with elevated Ti contents (~0.15 apfu), which occur in association with titanium oxides such as rutile and ilmenite (see Table 3; Cotkin, 1987; Henry and Dutrow, 1996), which might suggest blueschist facies. Opposing this interpretation is the lack of mineral indicators for these P-T ranges, such as glaucophane or omphacite in the HMAs analysed. On the other hand, their absence may be due to the higher susceptibility of amphiboles and pyroxenes to chemical and physical weathering, or if these minerals were not present in or were removed from the source materials before these fed the Szozdy Delta.

DEEP BURIAL VS. SURFACE WEATHERING OVERPRINTS IN THE SOURCE AREA – DISCUSSION

According to previously accepted sedimentological and burial models (e.g., Kutek and Głazek, 1972; Świdrowska et al., 2008), the present-day San Anticlinorium was located in the axial, most rapidly subsiding part of the Polish Basin, i.e. the Mid-Polish Trough. Consequently, this area was therefore traditionally considered to be deeply buried by Mesozoic deposits. In contrast to this proposed framework is a bathymetric model, combined with a palaeotectonic evolution model of the Lower San Anticlinorium (Remin et al., 2022a), that proposes an alternative view. This model indicates (during the late Cretaceous) the presence of an elevated area in the place of the subsurface Lower San Anticlinorium, i.e. Łysogóry-Dobrogea Land, instead of the deepest part of the basin. This landmass, located to the south of the present-day Roztocze Hills, supplied material to the developing Szozdy Delta System. Accordingly, deep burial was unlikely to have occurred (Remin et al., 2022a), which seems to be supported by the heavy mineral data analysed in this study.

Despite the well-known phenomenon of significant clastic input into the Late Cretaceous deposits of the Roztocze Hills, the origin of the parent rocks and the potential degree of burial have not been thoroughly investigated. Analysis of heavy mineral assemblages from the Szozdy Delta System reveals their distinctly polycyclic nature. High ZTR index values (zircon, tourmaline, rutile), a high degree of roundness, and the presence of abraded features suggest multiple episodes of redeposition. However, the occurrence of predominantly angular grains of

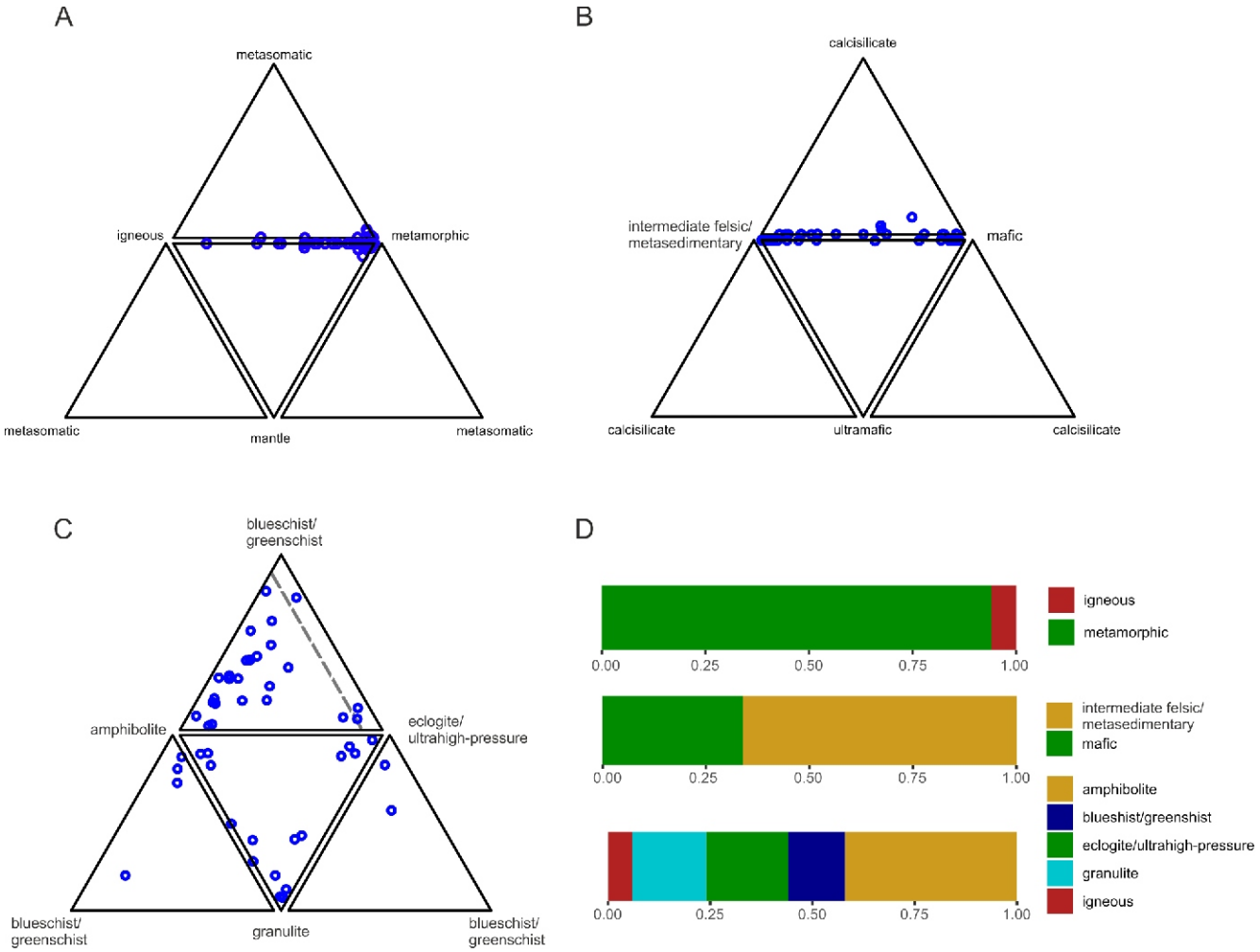

Fig. 16. Garnet discrimination schemes: (A) rock setting, (B) host-rock composition;,(C) metamorphic facies, (D) barplot showing the corresponding class assignment

Made with garnetRF (Schönig et al., 2021)

minerals less resistant to erosion contradicts the idea of repeated redeposition. Accordingly, the data suggest the presence of two distinct sources, The first source delivered multi-recycled mineral phases, dominated by the ZTR group minerals, likely derived from unmetamorphosed siliciclastic or metapelites/metapsammites (e.g., regenerated zoned tourmalines). The second, a “fresh” source, provided angular garnet, kyanite, and staurolite grains, indicating metamorphosed rocks as the main source. Alternatively, the relatively restricted diversity of heavy minerals, especially the almost total lack of apatites, pyroxenes and amphiboles, may result from the original impoverishment of the source rocks in these mineral phases before their deposition and further exhumation. Alternatively, they may have been removed by chemical weathering in a hot and humid climate, and this scenario is preferred by the authors because of the arguments given below.

Such HMA characteristics would be difficult (or impossible) to obtain from the suggested Mesozoic sedimentary cover of the Lower San Anticlinorium (if a Mesozoic cover was even present), suggesting the need to explore alternative sources. In light of these data, the most logical source is the Neoproterozoic-Cambrian basement of the Lower San Anticlinorium (beneath the Miocene cover of the Carpathians Foredeep), as we previously suggested (Remin et al., 2022a). In this area, both unmetamorphosed and metamorphosed deposits are present, forming the basement of the Małopolska Block as represented by flysch-like deposits (e.g., Żelaźniewicz et al., 2009, 2011; Buła and Habryn, 2011). Most likely, these rocks were already exposed and eroded during the late Cretaceous.

There may be several reasons for the low mineralogical diversity of the HMAs. Firstly, the diversity may be controlled to a large extent by the composition of the source rocks (Garzanti and Andò, 2007). Secondly, it may result from the diagenetic leaching of labile minerals (Morton and Hallsworth, 2007). The leaching of labile pyroxenes can already proceed at depths as little as several tens of metres (Milliken, 2007; Morton and Hallsworth, 2007; Garzanti et al., 2018). According to Garzanti et al. (2018), at depths not exceeding 1.5 km, transparent heavy minerals account for no more than 20% of the original assemblages. In overburdens of 1.5–2.5 km, the heavy mineral suites constitute ~5% of the original composition and only 1% if burial depths exceed 4.5 km. Thirdly, the low diversity of heavy mineral suites may result from weathering in acidic soils (Lång, 2000; Van Loon and Mange, 2007; Shaetzl and Thompson, 2015; Woronko et al., 2022). Chemical decomposition is associated with prolonged hydrolysis leading to the breakdown of labile minerals (Garzanti, 2017). It is strongly dependent on cli-

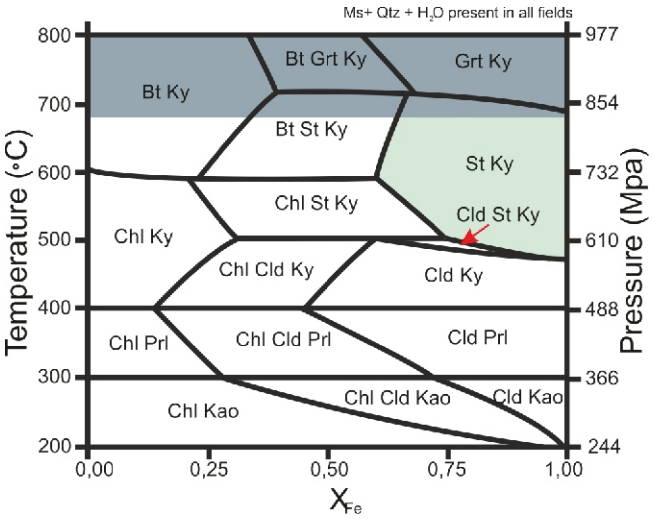

Fig. 17. Fe–Mg dependence of the stable assemblage distribution in the KFMASH system along a kyanite-type geotherm (continent-collision type metamorphism)

The grey shaded area above 680°C marks the region where muscovite melts and is no longer present in the assemblage fields. In very Mg-rich metapelites, chlorite-kyanite does not decompose before the middle amphibolite facies is reached (600°C), and the highest grade assemblage is phlogopite ţ-kyanite; scheme adapted from Bucher and Frey (2002). Abbreviations: Bt – biotite; Ky – kyanite; Grt – garnet; St – staurolite; chl – chlorite; Cld – chloritoid; Prl – pyrophyllite; Kao – kaolinite

matic conditions, rock porosity and permeability, water quality, and the chemical composition of the decomposing rock, often in combination.

Accordingly, extensive chemical weathering of the parental rocks in the surface conditions just before or during alluvial storage in the Szozdy Delta System might be responsible for the almost complete lack (by removal) of apatite (the few grains present display dissolution structures). A similar situation is likely applicable to garnets, as their abundance is much lower than that of the durable ZTR group minerals. Additionally, ~50% of garnets are heavily corroded. As both these mineral phases are durable in burial diagenesis (Velbel, 1984; Bateman and Catt, 1985; Morton and Hallsworth, 1999), the weathering conditions noted above are suggested to be responsible for their marked depletion in the HMAs of the section studied. Accordingly, either the garnets were derived from a different source than the ZTR group minerals, or the source rocks were originally depleted in these mineral phases.

Additionally, the garnet grains show dissolution structures, such as etch pits and polygonal and flat tops of mammillary features (Fig. 18). These widely understood structures are known from Quaternary deposits and saprolites, and are related to the action of humic acids formed during pedogenesis (Velbel, 1984; Hansley and Briggs, 1994). The dissolution structures observed on garnet grains cannot be inherited, because the fragile forms of heavily corroded garnets would break down as a result of intense wave and/or current action (Van Loon and Mange, 2007).

As such, the unique fragility of the corroded garnets rules out the possibility of multi-stage recycling. The presence of weathered garnets with altered surface structures suggests that the source rocks experienced significant surface weathering during Cretaceous times. This also indicates that the transport of garnet grains from weathered and exposed sediments was very limited (brief), preventing their destruction during transportation, ultimately leading to their deposition on the Szozdy Delta.

This burial/weathering interpretation is also corroborated by the absence of faceted garnets in the Szozdy section. Faceted garnets are known from many deeply buried basins around the world, including the central North Sea, offshore New Zealand, and New Mexico (Hansley, 1987). Faceted garnets form as a result of increased pore fluid temperatures (Morton et al.,

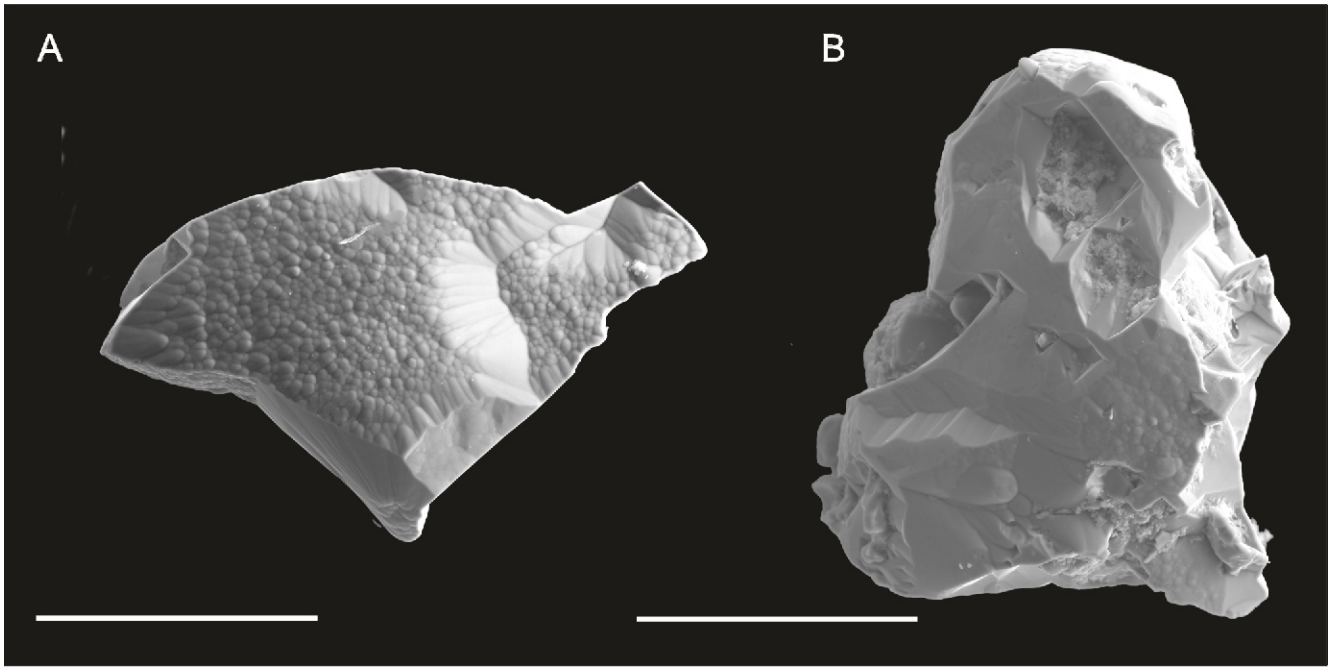

Fig. 18. Examples of garnets with etched surfaces from the Szozdy section: (A) – garnet with polygonal mammillary structure; (B) – garnet with smooth and etched surface, with initial mammillary structures and etch pits

Scale bars 100 μm

1989). According to Hansley (1987), sulphate-rich fluids at temperatures of 100–130°C are responsible for the creation of garnets with angular surfaces in the Upper Jurassic Morrison Formation of northwestern New Mexico. Faceted garnets do not occur in soil sections in modern sediments (Morton et al., 1989).

The exposed Neoproterozoic-Cambrian unmetamorphosed and metamorphosed basement rocks of the San Anticlinorium, represented by flysch-like deposits, were most likely subjected to intense surface weathering during the Late Cretaceous. Such a scenario is independently supported by the climatic conditions inferred from plant community analyses based on fossil leaves (Halamski, 2012). The abundant vegetation, and high humidity and temperature, intensified the humic acid-mediated dissolution of labile minerals, most likely removing them from the mineral assemblages analysed, resulting in the specific, low-diversity characteristics of the HMAs we obtained.

SUMMARY AND FUTURE NEEDS

1. Heavy mineral analysis of the Upper Cretaceous siliciclastic strata of the Roztocze Hills shows clearly bipartite mineral assemblages. These include mostly well-rounded zircons, tourmalines, and rutiles (ultrastable mineral phases) which might suggest multirecycling. By contrast, angular garnets, kyanites, staurolites, and sillimanites, preclude multi-stage recycling. It seems that one deposit was "old", repeatedly redeposited and subject to long-term weathering (ZTR group minerals). The second type of parental rocks was "fresh", most likely metamorphic, and subjected to extremely effective surface weathering, as demonstrated by the characteristic structures found on the garnets and staurolites. Minerals particularly susceptible to chemical weathering, such as apatite (whose existence is almost exclusively confined to inclusions in tourmalines), amphiboles, and pyroxenes, were completely removed from the heavy mineral assemblages during extensive Cretaceous weathering, or simply the parental rocks were originally depleted in these mineral phases before they were deposited.

2. The most logical source rocks for the heavy mineral assemblages of the Szozdy Delta System are thought to be the Neoproterozoic-Cambrian basement of the present-day area of the Lower San Anticlinorium (part of the Małopolska Block).

3. Weathering structures are especially prominent on garnets and staurolites. Mammillary structures observed on garnets and staurolites emphasize the importance of surface weathering overprints. Apatite traces (single crystals, inclusions within tourmalines) suggest that apatite grains were almost entirely eliminated during Cretaceous pedogenic/alluvial storage processes. Lush vegetation, hot and humid climate conditions, and acidic soil pH effectively eliminated apatite and were responsible for the origination of the weathering structures present on garnet and staurolite grains.

4. The composition of heavy mineral assemblages was undoubtedly influenced by hydrodynamic processes such as selective grain entrainment, transport, and grain settling velocities. This is particularly highlighted by oscillations in the RuT index (rutile and tourmaline), emphasizing the differences between the heavy mineral assemblages of the distal and proximal facies of the delta system.

5. The presence of regenerated tourmaline grains that rebuilt their idiomorphic shape on former round tourmaline nuclei indicates original greenschist to amphibolite facies conditions.

6. The outer rims of zoned tourmalines are derived from Al-rich metapelites type 1, which correspond to tourmalines originating from metapelites in equilibrium with aluminous minerals such as staurolite and kyanite, like most homogeneous tourmalines. The centres of zoned grains are most likely of igneous origin – granitoid types 1 and 3 (Henry and Guidotti, 1985).

7. The source rocks for the garnet groups are predominantly schists, ortho-gneisses, para-gneisses, and amphibolites, formed under pressure-temperature conditions transitional between granulite and amphibolite facies, as well as between amphibolite and greenschist facies. The genesis of most of the garnet grains studied is likely linked to metasedimentary rocks.The garnet RF classification scheme showed that a large majority of the garnets studied originated from intermediate felsic-metamorphic rocks. Most grains originate from rocks metamorphosed under amphibolite facies conditions.

8. Further research will concentrate on analyzing the spectra of radiometric ages of zircons extracted from the Szozdy Delta System, to constrain the ages of the eroded rocks and address the issue of the potential history and extent of burial, if any, of Łysogóry-Dobrogea Land during the Late Cretaceous.

Financial support. This research was supported by the Polish National Science Centre [Narodowe Centrum Nauki, Polska], under grant number – UMO-2018/29/B/ST10/02947; "*Late Cretaceous tectonic evolution of the SE part of the Danish-Polish Trough; revision of the facial architecture and implication for the paleo- and paleobiogeography of Europe*".

Acknowledgements. Our thanks are extended to Bartosz Gościmski, Joanna Roszkowska-Remin and Martyna Cyglicka for help during the fieldwork. The authors are grateful to the reviewers, two anonymous and Krzysztof Leszczyński (Polish Geological Institute – Polish Research Institute), whose suggestions and remarks markedly improved the final version of the manuscript. Thanks go to Jordan Todes (University of Chicago, USA) and Jan Zalasiewicz (University of Leicester) who kindly provided the linguistic improvement of the manuscript.

REFERENCES

Andò, S., Garzanti, E., Padoan, M., Limonta, M., 2012. Corrosion of heavy minerals during weathering and diagenesis: A catalog for optical analysis. Sedimentary Geology, **280**: 165–178; https://doi.org/10.1016/j.sedgeo.2012.03.023

Aubrecht, R., Meres, S., Sýkora, M., Mikus, T., 2009. Provenance of the detrital garnets and spinels from the Albian sediments of the Czorsztyn Unit (Pieniny Klippen Belt, Western Carpathians, Slovakia). Geologica Carpathica, **60**: 463–483; https://doi.org/10.2478/v10096-009-0034-z

Bateman, R.M., Catt, J.A., 1985. Modification of heavy mineral assemblages in English coversands by acid pedochemical weathering. Catena, **12**: 1–21; https://doi.org/10.1016/S0341-8162(85)80001-1

Baxter, E.F., Caddick, M.J., Ague, J.J., 2013. Garnet: common mineral, uncommonly useful. Elements, **9**: 415–419; https://doi.org/10.2113/gselements.9.6.415

Błaszkiewicz, A., 1980. Campanian and Maastrichtian ammonites of the Middle Vistula River Valley, Poland: a stratigraphic-palaeontological study. Prace Instytutu Geologicznego, **92**: 3–63.

Breiman, L., 2001. Random forests. Machine Learning, **45**: 5–32; https://doi.org/10.1023/A:1010933404324

Bucher, K., Frey, M., 2002. Petrogenesis of Metamorphic Rocks. Springer Science & Business Media; https://doi.org/10.1007/978-3-540-74169-5

Buła, Z., Habryn, R., 2011. Precambrian and Palaeozoic basement of the Carpathian Foredeep and the adjacent Outer Carpathians (SE Poland and western Ukraine). Annales Societatis Geologorum Poloniae, **81**: 221–239.

Buła, Z., Byś, I., Florek, R., Habryn, R., Jachowicz, M., Kwarciński, J., Laskowicz, R., Liszka, B., Madej, K., Maksym, A., Markowiak, M., Pietrusiak, M., Probulski, J., Ryłko, W., Salwa, S., Sikora, R., Staryszak, G., Tabol-Wójcik, P., Tomaś, A., Zacharski, J., 2008. Geological-Structural Atlas of the Palaeozoic Basement of the Outer Carpathians and Carpathian Foredeep. Państwowy Instytut Geologiczny, Warszawa.

Cotkin, S.J., 1987. Conditions of metamorphism in an early Paleozoic blueschist schist of Skookum Gulch, northern California. Contributions to Mineralogy and Petrology, **96**: 192–200; https://doi.org/10.1007/BF00375233

Cyglicki, M., Remin, Z., 2023. Rutile to tourmaline index – a tool for the recognition of the hydrodynamics of the depositional environment; a case study from the Campanian Szozdy Delta System, SE Poland. Acta Geologica Polonica, **63**: 833–851; https://doi.org/10.2445/agp.2023.148025

Dadlez, R., Narkiewicz, M., Stephenson, R.A. Visser, M.T.M., van Wess, J.D., 1995. Tectonic evolution of the Mid-Polish Trough: modelling implications and significance for central European geology. Tectonophysics, **252**: 179–195; https://doi.org/10.1016/0040-1951(95)00104-2

Dadlez, R., Marek, S., Pokorski, J. (eds.), 1998. Palaeographical Atlas of the Epicontinental Permian and Mesozoic in Poland (1:2,500,000). Polish Geological Institute, Warszawa.

Dadlez, R., Marek, S., Pokorski, J. (eds), 2000. Geological Map of Poland without Cenozoic Deposits at 1:1,000,000 Scale. Polish Geological Institute, Warszawa.

Dietz, V., 1973. Experiments on the influence of transport on shape and roundness of heavy minerals. Contributions to Sedimentology, **1:** 69–102.

Dziadzio, P., Jachowicz, M., 1996. Geological structure of the Miocene substrate SW of the Lubaczów Uplift (SE Poland) (in Polish with English summary). Przegląd Geologiczny, **44**: 1124–1130.

Dziadzio, P., Maksym, A., Olszewska, B., 2006. Miocene deposition in the eastern part of the Carpathian Foredeep in Poland (in Polish with English summary). Przegląd Geologiczny, **54**: 413–420.

Dubicka, Z., 2015. Benthic foraminiferal biostratigraphy of the lower and middle Campanian of the Polish Lowlands and its application for interregional correlation. Cretaceous Research, 56: 491–503; https://doi.org/10.1016/j.cretres.2015.06.012

Dubicka, Z., Peryt, D., Szuszkiewicz, M., 2014. Foraminiferal evidence for paleogeographic and paleoenvironmental changes across the Coniacian-Santonian boundary in western Ukraine. Palaeogeography, Palaeoclimatology, Palaeoecology, **401**: 43–56; https://doi.org/10.1016/j.palaeo.2014.03.002

Freise, F.W., 1931. Untersuchung von mineralen auf Abnutzbarkeit bei Verfrachtung im Wasser. Zeitschrift für Kristallographie, Mineralogie und Petrographie, **41**: 1–7.

Garzanti, E., 2017. The maturity myth in sedimentology and provenance analysis. Journal of Sedimentary Research, **87**: 353–365; https://doi.org/10.2110/jsr.2017.17

Garzanti, E., Andò, S., 2007. Heavy mineral concentration in modern sands: implications for provenance interpretation. Developments in Sedimentology, **58**: 517–545; https://doi.org/10.1016/S0070-4571(07)58020-9

Garzanti, E., Andò, S., 2019. Heavy minerals for Junior Woodchucks. Minerals, **9**, 148; https://doi.org/10.3390/min9030148

Garzanti, E., Andò, S., Limonta, M., Fielding, L., Najman, Y., 2018. Diagenetic control on mineralogical suites in sand, silt, and mud (Cenozoic Nile Delta): Implications for provenance reconstructions. Earth-Science Reviews, **185**: 122–139; https://doi.org/10.1016/j.earscirev.2018.05.010

Hakenberg, M., Świdrowska, J., 1998. Evolution of the Holy Cross segment of the Mid-Polish Trough during the Cretaceous. Geological Quarterly, **42** (3): 239–262.

Hakenberg, M., Świdrowska, J., 2001. Cretaceous basin evolution in the Lublin area along the Teisseyre-Tornquist Zone (SE Poland). Annales Societatis Geologorum Poloniae, **71**: 1–20.

Halamski, A.T., 2012. Latest Cretaceous leaf floras from Southern Poland and Western Ukraine. Acta Palaeontologica Polonica, **58**: 407–433; https://doi.org/10.4202/app.2011.0024

Hansley, P.L., 1987. Petrologic and experimental evidence for the etching of garnets by organic acids in the Upper Jurassic Morrison Formation, northwestern New Mexico. Journal of Sedimentary Petrology Research, **57**: 666–681; https://doi.org/10.1306/212F8BCF-2B24-11D7-8648000102C1865D

Hansley, P.L., Briggs, P.H., 1994. Garnet Dissolution in Oxalic Acid – a Possible Analog for Natural Etching of Garnet by Dissolved Organic Matter (No. 2106). US Government Printing Office; https://doi.org/10.3133/b2106

Henry, D.J., Dutrow, B.L., 1992. Tourmaline in a low grade clastic metasedimentary rock: an example of the petrogenetic potential of tourmaline. Contributions to Mineralogy and Petrology, **112**: 203–218; https://doi.org/10.1007/BF00310455

Henry, D.J., Dutrow, B.L., 1996. Metamorphic tourmaline and its petrologic applications. Reviews in Mineralogy, **33**: 503–557.

Henry, D.J., Dutrow, B.L., 2012. Tourmaline at diagenetic to low-grade metamorphic conditions: its petrologic applicability. Lithos, **154**: 16–32; https://doi.org/10.1016/j.lithos.2012.08.013

Henry, D.J., Guidotti, C.V., 1985. Tourmaline as a petrogenetic indicator mineral: an example from the staurolite-grade metapelites of NW Maine. American Mineralogist, **70**: 1–15.

Hubert, J.F., 1962. A zircon-tourmaline-rutile maturity index and interdependence of the composition of heavy mineral assemblages with the gross composition and textures of sandstones. Journal of Sedimentary Petrology Research, **32**: 440–450; https://doi.org/10.1306/74D70CE5-2B21-11D7-8648000102C1865D

Jaskowiak-Schoeneichowa, M., Krassowska, A., 1988. Palaeothickness, lithofacies and palaeotectonics of the epicontinental Upper Cretaceous in Poland (in Polish with English summary). Geological Quarterly, **32** (1): 177–198.

Jones, B.G., Cart, P.F., Condliffe, E., 1981. Ferrian tourmaline from Bungonia, New South Wales. Journal of the Geological Society of Australia, **28**: 13–17.

Jurkowska, A., Barski, M., 2017. Maastrichtian island in the Central European Basin-new data inferred from palynofacies analysis and inoceramid stratigraphy. Facies, **63**: 1–20; https://doi.org/10.1007/s10347-017-0509-9

Jurkowska, A., Barski, M., Worobiec, E., 2019a. The relation of a coastal environment to early diagenetic clinoptilolite (zeolite) formation-New data from the Late Cretaceous European Basin. Palaeogeography, Palaeoclimatology, Palaeoecology, **524**: 166–182; https://doi.org/10.1016/j.palaeo.2019.03.025

Jurkowska, A., Świerczewska-Gładysz, E., Bąk, M., Kowalik, S., 2019b. The role of biogenic silica in the formation of Upper Cretaceous pelagic carbonates and its palaeoecological implications. Cretaceous Research, **93**: 170–187; https://doi.org/10.1016/j.cretres.2018.09.009

Kamieński, M., 1925. Contribution a la connaissance du facies Sablonneux des cauches crétacèes de Żurawno (Pologne) (in Polish with French summary). Kosmos, **50**: 1408–1425.

Kley, J., Voigt, T., 2008. Late Cretaceous intraplate thrusting in Central Europe: Effect of Africa-Iberia-Europe convergence, not Alpine collision. Geology, **36**: 839–842; https://doi.org/10.1130/G24930A.1

Komar, P.D., 2007. The entrainment, transport and sorting of heavy minerals by waves and currents. Developments in Sedimentology, **58**: 3–48; https://doi.org/10.1016/S0070-4571(07)58001-5

Kowalska, S., Kranc, A., Maksym, A., Śmist, P., 2000. Geology of the north-eastern part of the Carpathian Foredeep basement, the Lubaczów-Biszcza Region. Nafta-Gaz (in Polish), **54**: 158–178.

Krassowska, A., 1997. Kreda górna. Sedymentacja, paleogeografia i paleotektonika (in Polish). Prace Państwowego Instytutu Geologicznego, **153**: 386–402.

Krumbein, W.C., 1941. Measurement and geological significance of shape and roundness of sedimentary particles. Journal of Sedimentary Petrology Research, **11**: 64–72; https://doi.org/10.1306/D42690F3-2B26-11D7-8648000102C1865D

Krynine, P.D., 1946. The tourmaline group in sediments. The Journal of Geology, **54**: 65–87; https://doi.org/10.1086/625323

Krzywiec, P., 1999. Miocene tectonic evolution of the Eastern Carpathian Foredeep Basin (Przemyśl–Lubaczów) in light of seismic data interpretation (in Polish with English summary). Prace Państwowego Instytutu Geologicznego, **168**: 249–276.

Krzywiec, P., 2000. On mechanism of the Mid-Polish Trough inversion (in Polish with English summary). Biuletyn Państwowego Instytutu Geologicznego, **393**: 135–166.

Krzywiec, P., 2002. Mid-Polish Trough inversion – seismic examples, main mechanisms and its relationship to the Alpine Carpathian collision. Continental collision and the tectono-sedimentary evolution of forelands. European Geophysical Society Special Publication, **1**: 151–165.

Krzywiec, P., 2006. Structural inversion of the Pomeranian and Kuiavian segments of the Mid-Polish Trough–lateral variations in timing and structural style. Geological Quarterly, **50** (1): 151–168.

Krzywiec, P., 2009. Devonian–Cretaceous repeated subsidence and uplift along the Teisseyre–Tornquist zone in SE Poland – insight from seismic data interpretation. Tectonophysics, **475**: 142–159; https://doi.org/10.1016/j.tecto.2008.11.020

Krzywiec, P., Stachowska, A., 2016. Late Cretaceous inversion of the NW segment of the Mid-Polish Trough – how marginal troughs were formed, and does it matter at all? Zeitschrift der Deutschen Gesellschaft für Geowissenschaften, **167**: 107–119; https://doi.org/10.1127/zdgg/2016/0068

Krzywiec, P., Gutkowski, J., Walaszczyk, I., Wróbel, G., Wybraniec, S., 2009. Tectonostratigraphic model of the Late Cretaceous-inversion along the Nowe Miasto–Zawichost fault zone, SE Mid-Polish Trough. Geological Quarterly, **53** (1): 27–48.

Krzywiec, P., Stachowska, A., Stypa, A., 2018. The only way is up–on Mesozoic uplifts and basin inversion events in SE Poland. Geological Society Special Publications**, 469:** 33–57; https://doi.org/10.1144/SP469.14

Kutek, J., Głazek, J., 1972. The Holy Cross area, Central Poland, in the Alpine cycle. Acta Geologica Polonica, **22**: 603–652.

Lång, L.O., 2000. Heavy mineral weathering under acidic soil conditions. Applied Geochemistry, **15**: 415–423; https://doi.org/10.1016/S0883-2927(99)00064-5

Leszczyński, K., 2010. Lithofacies evolution of the Late Cretaceous basin in the Polish Lowlands (in Polish with English summary). Biuletyn Państwowego Instytutu Geologicznego, **443**: 33–54.

Leszczyński, K., 2012. The internal geometry and lithofacies pattern of the Upper Cretaceous–Danian sequence in the Polish Lowlands. Geological Quarterly, **56** (2): 363–386.

Leszczyński, K., Dadlez, R. 1999. Subsidence and the problem of incipient inversion in the Mid-Polish Trough based on thickness maps and Cretaceous lithofacies analysis – discussion (in Polish with English summary). Przegląd Geologiczny, **47**: 625–628.

Locock, A.J., 2008. An Excel spreadsheet to recast analyses of garnet into end-member components, and a synopsis of the crystal chemistry of natural silicate garnets. Computers & Geosciences, **34**: 1769–1780.

Łuszczak, K., Wyglądała, M., Śmigielski, M., Waliczek, M., Matyja, B.A., Konon, A., Ludwiniak, M., 2020. How to deal with missing overburden – investigating exhumation of the fragment of the Mid-Polish Anticlinorium by a multi-proxy approach. Marine and Petroleum Geology, **114**: 104–229; https://doi.org/10.1016/S0341-8162(85)80001-1

Mange, M.A., Maurer, H.F.W., 1992. Heavy Mineral in Colour. Chapman and Hall, London.

Mange, M.A., Morton, A.C., 2007. Geochemistry of heavy minerals. Developments in Sedimentology, **58**: 345–391; https://doi.org/10.1016/S0070-4571(07)58013-1

Mange-Rajetzky, M.A., 1995. Subdivision and correlation of monotonous sandstone sequences using high resolution heavy mineral analysis, a case study: the Triassic of the Central Graben. Geological Society Special Publications, **89**: 23–30; https://doi.org/10.1144/GSL.SP.1995.089.01.03

Meres, Š., 2008. Garnets – important information resource about source area and parental rocks of the siliciclastic sedimentary rocks (in Slovak with English summary). In: Conference "Cambelove dni 2008" (ed. L. Jurkovič): 37–43. Comenius University, Bratislava.

Milliken, K.L., 2007. Provenance and diagenesis of heavy minerals, Cenozoic units of the northwestern Gulf of Mexico sedimentary basin. Developments in Sedimentology, **58**: 247–261; https://doi.org/10.1016/S0070-4571(07)58008-8

Morton, A.C., Hallsworth, C., 1994. Identifying provenance-specific features of detrital heavy mineral assemblages in sandstones. Sedimentary Geology, **90**: 241–256; https://doi.org/10.1016/0037-0738(94)90041-8

Morton, A.C., Hallsworth, C., 1999. Processes controlling the composition of heavy mineral assemblages in sandstones. Sedimentary Geology**, 124**: 3–29; https://doi.org/10.1016/S0037-0738(98)00118-3

Morton, A.C., Hallsworth, C., 2007. Stability of detrital heavy minerals during burial diagenesis. Developments in Sedimentology, **58**: 215–245; https://doi.org/10.1016/S0070-4571(07)58007-6

Morton, A.C., Borg, G., Hansley, P.L., Haughton, P.D.W., Krinsley, D.H., Trusty, P., 1989. The origin of faceted garnets in sandstones: dissolution or overgrowth? Sedimentology, **36**: 927–942; https://doi.org/10.1111/j.1365-3091.1989.tb01754.x

Narkiewicz, M., Petecki, Z., 2017. Basement structure of the Paleozoic Platform in Poland. Geological Quarterly, **61** (2): 502–520; https://doi.org/10.7306/gq.1356

Narkiewicz, M., Maksym, A., Malinowski, M., Grad, M., Guterch, A., Petecki, Z., Probulski, J., Janik, T., Majdański, M., Środa, P., Czuba, W., Gaczyński, E., Jankowski, L., 2015. Transcurrent nature of the Teisseyre–Tornquist Zone in Central Europe: results of the POLCRUST-01 deep reflection seismic profile. International Journal of Earth Sciences, **104**: 775–796; https://doi.org/10.1007/s00531-014-1116-4

Nielsen, S.B., Hansen, D.L. 2000. Physical explanation of the formation and evolution of inversion zones and marginal troughs. Geology, **28**: 875–878; https://doi.org/10.1130/0091-7613(2000)28<875:PEOTFA>2.0.CO;2

Nowak, J., 1907. Przyczynek do znajomości kredy Lwowsko-Rawskiego Roztocza (in Polish). Kosmos, **32**: 160–169.

Nowak, J., 1908. Spostrzeżenia w sprawie wieku kredy zachodniego Podola (in Polish). Kosmos, **33**: 279–285.

Odin, G.S., Lamaurelle, M.A., 2001. The global Campanian-Maastrichtian stage boundary. Episodes, **24**: 229–238.

Olszewska, D., 1990. Belemnites from the Upper Cretaceous chalk of Mielnik (eastern Poland). Acta Geologica Polonica, **40**: 111–128.

Pasternak, S.I., 1959. Biostratygrafiya kreydovykh vidkladiv Volyno-Podilskoi plyty (in Ukrainian), Akademia Nauk Ukrainskoi RSR, Kyiv.

Pasternak, S.I., Gavrylyshyn, V.I., Ginda, V.A., Kotsyubinsky, S.P., Senkovskyi, Y.M., 1968. Stratygrafia i fauna kredovykh vidkladiv zakhodu Ukrainy (in Ukrainian). Naukova Dumka, Kyiv.

Pasternak, S.I., Senkovskyi, Y.M., Gavrylyshyn, V.I., 1987. Volyno-Podillya u kreydovomu periodi (in Ukrainian). Naukova Dumka, Kyiv.

Povondra, P., Novak, M., 1986. Tourmalines in metamorphosed carbonate rocks from western Moravia, Czechoslovakia. Neues Jahrbuch für Mineralogie Monatshefte: 273–282.

Powers, M.C., 1953. A new roundness scale for sedimentary particles. Journal of Sedimentary Petrology Research, **23**: 117–119; https://doi.org/10.1306/D4269567-2B26-11D7-8648000102C1865D

Pożaryski, W., 1956. Kreda (in Polish). In: Regionalna Geologia Polski, 2 (eds. M. Książkiewicz and S. Dżułyński). Polskie Towarzystwo Geologiczne, Państwowe Wydawnictwo Naukowe, Kraków.

Pożaryski, W., 1960. An outline of the stratigraphy and palaeogeography of the Cretaceous in the Polish Lowland (in Polish with English summary). Prace Instytutu Geologicznego, **30**: 377–418.

Pożaryski, W., 1962. Kreda (in Polish). Atlas geologiczny Polski. Zagadnienia stratygraficzno-facjalne. Instytut Geologiczny, Warszawa.

Pożaryski, W., 1974. Tectonics. Part 1. Polish Lowlands. In: Geology of Poland, IV (ed. W. Pożaryski): 2–34. Wyd. Geol., Warszawa.

Remin, **Z.**, **2012**. The Belemnella stratigraphy of the Campanian-Maastrichtian boundary; a new methodological and taxonomic approach. Acta Geologica Polonica, **62**: 495–533; https://doi.org/10.2478/V10263-012-0028-5

Remin, Z., 2015. The Belemnitella stratigraphy of the Upper Campanian–basal Maastrichtian of the Middle Vistula section, central Poland. Geological Quarterly, **59** (4): 783–813; https://doi.org/10.7306/gq.1257

Remin, Z., 2018. Understanding coleoid migration patterns between eastern and western Europe–belemnite faunas from the upper lower Maastrichtian of Hrebenne, southeast Poland. Cretaceous Research, **87**: 368–384; https://doi.org/10.1016/j.cretres.2017.06.010

Remin, Z., Dubicka, Z., Kozłowska, A., Kuchta, B., 2012. A new method of rock disintegration and foraminiferal extraction with the use of liquid nitrogen [LN2]. Do conventional methods lead to biased paleoecological and paleoenvironmental interpretations? Marine Micropaleontology, **86**: 11–14; https://doi.org/10.1016/j.marmicro.2011.12.001

Remin, Z., Cyglicki, M., Cybula, M., Roszkowska-Remin, J., 2015a. Deep versus shallow? Deltaically influenced sedimentation and new transport directions – case study from the Upper Campanian of the Roztocze Hills, SE Poland. In: Proceedings of the 31st IAS Meeting of Sedimentology: 438. Kraków, Poland.

Remin, Z., Machalski, M., Jagt, J.W.M., 2015b. The stratigraphically earliest record of *Diplomoceras cylindraceum* (heteromorph ammonite) – implications for Campanian/Maastrichtian boundary definition. Geological Quarterly, **59** (4): 843–848; https://doi.org/10.7306/gq.1253

Remin, Z., Gruszczyński, M. Marshall, J., 2016. Changes in paleo-circulation and the distribution of ammonite faunas at the Coniacian–Santonian transition in central Poland and western Ukraine. Acta Geologica Polonica, **66**: 107–124; https://doi.org/10.1515/agp-2016-0006

Remin, Z., Cyglicki, M., Niechwedowicz, M., 2022a. Deep vs. shallow – two contrasting theories? A tectonically activated Late Cretaceous deltaic system in the axial part of the Mid-Polish Trough: a case study from southeast Poland. Solid Earth, **13**: 681–703; https://doi.org/10.5194/se-13-681-2022

Remin, Z., Krzywiec, P., Stachowska, A., 2022b. Late Cretaceous inversion of SE Polish Basin – syn-depositional tectonics, facies distribution and bathymetric changes. In: Cretaceous of Poland and of adjacent areas (eds. I. Walaszczyk and J. Todes), Field trip Guides: 87–114. Faculty of Geology, University of Warsaw, Warsaw.

Resak, M., Narkiewicz, M., Littke, R., 2008. New basin modeling results from the Polish part of the Central European Basin system: implications for the Late Cretaceous–Early Paleogene structural inversion. International Journal of Earth Sciences, **97**: 955–972; https://doi.org/10.1007/s00531-007-0246-3

Rogala, W., 1909. O stratygrafii utworów kredowych Podola (in Polish). Kosmos, **34**: 1160–1164.

Ryan, P.D., Mange, M.A., Dewey, J.F., 2007. Statistical analysis of high-resolution heavy minerals stratigraphic data from Ordovician of western Ireland and its tectonic consequences. Developments in Sedimentology, **58**: 465–489; https://doi.org/10.1016/S0070-4571(07)58018-0

Samsonowicz, J., 1925. Esquisse géologique des environs de Rachów sur la Vistule et les transgressions de l'Albien et du Cénomanien dans le sillon nord-européen (in Polish with French summary). Sprawozdania Państwowego Instytutu Geologicznego, **3**: 45–118.

Schaetzl, R.J., Thomson, M.L., 2015. Soils: Genesis and Geomorphology. Cambridge University Press.

Schönig, J., von Eynatten, H., Tolosana-Delgado, R., Meinhold, G., 2021. Garnet major-element composition as an indicator of host-rock type: a machine learning approach using the random forest classifier. Contributions to Mineralogy and Petrology, **176**: 1–21; https://doi.org/10.1007/s00410-021-01854-w

Sperlich, R., Giere, R., Frey, M., 1996. Evolution of compositional polarity and zoning in tourmaline during prograde metamorphism of sedimentary rocks in the Swiss Central Alps. American Mineralogist, **81**: 1222–1236; https://doi.org/10.2138/am-1996-9-1021

Świdrowska, J., 2007. Cretaceous in Lublin area – sedimentation and tectonic conditions (in Polish with English summary). Biuletyn Państwowego Instytutu Geologicznego, **422**: 63–78.

Świdrowska, J., Hakenberg, M., 1999. Subsidence and the problem of incipient inversion in the Mid-Polish Trough based on thickness maps and Cretaceous lithofacies analysis (in Polish with English summary). Przegląd Geologiczny, **47**: 61–68.

Świdrowska, J., Hakenberg, M., Poluhtovič, B., Seghedi, A., Višnâkov, I., 2008. Evolution of the Mesozoic basins on the southwestern edge of the East European Craton (Poland, Ukraine, Moldova, Romania). Studia Geologica Polonica, **130**: 3–130.

Thiel, G.A., 1940. The relative resistance to abrasion of mineral grains of sand size. Journal of Sedimentary Petrology Research, **10**: 103–124; https://doi.org/10.1306/D42690A3-2B26-11D7-8648000102C1865D

Thiel, G.A., 1945. Mechanical effects of stream transportation of mineral grains of sand size. GSA Bulletin, **56**: 1207.

Van Loon, A.J., Mange, M.A., 2007. "In situ" dissolution of heavy minerals through extreme weathering, and the application of the surviving assemblages and their dissolution characteristics to correlation of Dutch and German Silver Sands. Developments in Sedimentology, **58**: 189–213; https://doi.org/10.1016/S0070-4571(07)58006-4

Velbel, M.A., 1984. Natural weathering mechanisms of almandine garnet. Geology, **12**: 631–634; https://doi.org/10.1130/0091-7613(1984)12<631:NWMOAG>2.0.CO;2

Velbel, M.A., 1999. Bond strength and the relative weathering rates of Simple orthosilicates. American Journal of Science, **299**: 679–696; https://doi.org/10.1130/0091-7613(1984)12<631:NWMOAG>2.0.CO;2

Voigt, T., Kley, J., Voigt, S., 2021. Dawn and dusk of Late Cretaceous basin inversion in Central Europe. Solid Earth, **12**: 1443–1471; https://doi.org/10.5194/se-12-1443-2021

Walaszczyk, I., 1992. Turonian through Santonian deposits of the Central Polish Upland; their facies development, inoceramid paleontology and stratigraphy. Acta Geologica Polonica, **42**: 1–122.

Walaszczyk, I., 2004. Inoceramids and inoceramid biostratigraphy of the Upper Campanian to basal Maastrichtian of the Middle Vistula River section, central Poland. Acta Geologica Polonica, **54**: 95–168.

Walaszczyk, I., Remin, Z., 2015. Kreda obrzeżenia Gór Świętokrzyskich (in Polish). In: Przewodnik LXXXIV Zjazdu Polskiego Towarzystwa Geologicznego, Chęciny: 41–50.

Walaszczyk, I., Dubicka, Z., Olszewska-Nejbert, D., Remin, Z., 2016. Integrated biostratigraphy of the Santonian through Maastrichtian (Upper Cretaceous) of extra-Carpathian Poland. Acta Geologica Polonica, **66**: 313–350; https://doi.org/10.1515/agp-2016-0016

Woronko, B., Zagórski, Z., Cyglicki, M., 2022. Soil-development differentiation across a glacial-interglacial cycle, Saalian upland, E Poland. Catena, **211**, 105968; https://doi.org/10.1016/j.catena.2021.105968

Yavuz, F., Karakaya, N., Yýldýrým, D.K., Karakaya, M.Ç., Kumral, M., 2014. A Windows program for calculation and classification of tourmaline-supergroup (IMA-2011). Computers & Geosciences, **63**: 70–87; https://doi.org/10.1016/j.cageo.2013.10.012

Ziegler, P.A., 1990. Geological Atlas of Western and Central Europe, 2nd Edition. Shell Internationale Petroleum Maatschappij, The Hague. Geological Society, London.

Żelaźniewicz, A., Buła, Z., Fanning, M., Seghedi, A., Żaba, J., 2009. More evidence on Neoproterozoic terranes in southern Poland and southeastern Romania. Geological Quarterly, **53** (1): 93–124.

Żelaźniewicz, A., Aleksandrowski, P., Buła, Z., Karnkowski, P., Konon, A., Oszczypko, N., Ślączka, A., Żaba, J., Żytko, K., 2011. Regionalizacja tektoniczna Polski (in Polish). Komitet Nauk Geologicznych, Wrocław. ISBN: 978-83-63377-01-4